Biomedical Physics &
Engineering Express

Endorsed by IPEM Institute of Physics and Engineering in Medicine
PURPOSE-LED PUBLISHING™

PAPER • **OPEN ACCESS**

Impact of metal nanoparticles on cell survival predicted by the local effect model for cells in suspension and tissue. Part 1: theoretical framework

To cite this article: Hans Rabus and Leo Thomas 2025 *Biomed. Phys. Eng. Express* **11** 065002

View the article online for updates and enhancements.

You may also like

- Tumor size dependent MNP dose evaluation in realistic breast tumor models for effective magnetic hyperthermia
Sandeep Nain, Neeraj Kumar and Pramod Kumar Avti
- Magnetic nanoparticles in nanomedicine: a review of recent advances
Kai Wu, Diqing Su, Jinming Liu et al.
- Retention assessment of magnetic nanoparticles in rat arteries with micro-computed tomography
Shu-Ju Tu, Siao-Yun Wu, Fu-Sheng Wang et al.





GAS

BreathSpec®

The combination of GC and IMS enables a physical separation to detect volatiles without pre-concentration directly sampled from human breath.

Our GC-IMS based analyzer allows instant breath sampling and analysis of volatiles in minutes.

The transportable GC-IMS facilitates versatile sampling incl. direct exhalation, syringe based and also gas bags for sampling of breath and static body headspace (oral/nasal/skin).

▶▶▶ click for more details

This content was downloaded from IP address 15.204.172.40 on 07/11/2026 at 09:09

Biomedical Physics & Engineering Express

Check for updates

OPEN ACCESS

RECEIVED
29 May 2026

ACCEPTED FOR PUBLICATION
18 June 2026

PUBLISHED
22 July 2026

Original content from this work may be used under the terms of the Creative Commons Attribution 4.0 licence.

Any further distribution of this work must maintain attribution to the author(s) and the title of the work, journal citation and DOI.

CORRIGENDUM

CORRIGENDUM: Impact of metal nanoparticles on cell survival predicted by the local effect model for cells in suspension and tissue: I. Theoretical framework (2025 *Biomed. Phys. Eng. Express* **11** 065002)

Hans Rabus[1,*] and **Leo Thomas**[1,2]

[1] Physikalisch-Technische Bundesanstalt, Berlin, Germany
[2] Technische Universität Berlin, Berlin, Germany
[*] Author to whom any correspondence should be addressed.

E-mail: hans.rabus@ptb.de

The authors regret that equation (A.4) on page 20 of the article contained a mistake. In the first case on the right-hand side, '$x_j \leqslant a-1 \leqslant x_i \leqslant a+1$' should read '$x_j \leqslant a-1$' so that the equation reads correctly as follows:

$$\overline{\omega}_2\left(r_i, r_j | R_c\right) = \begin{cases} \overline{\omega}_1\left(x_i | a\right) & x_j \leqslant a-1 \\ \overline{\omega}_2{}^{(3)}\left(x_i, x_j | a\right) & a-1 \leqslant x_j \leqslant 2a-x_i \ \wedge \ x_j \leqslant x_i \leqslant a+1 \\ \overline{\omega}_2{}^{(4)}\left(x_i, x_j | a\right) & 2a-x_i \leqslant x_j \leqslant x_i \leqslant a+1 \\ 0 & x_i \geqslant x_j > a+1 \end{cases} . \quad \text{(A.4)}$$

Owing to the error, the formula did not cover the case that both x_j and x_i are less or equal to $a-1$. In the code implementing the theory described in the paper, this case was correctly considered so that the results presented in the paper are not affected by the mistake and the conclusions of the paper remain unchanged.

The authors would like to apologise for any inconvenience caused.

Data availability statement

No new data were created or analysed in this study.

Author contributions

Hans Rabus 0000-0001-7700-9845
Writing – review & editing (lead)

Leo Thomas 0000-0002-2156-7298
Investigation (lead), Writing – review & editing (supporting)

© 2026 The Author(s). Published by IOP Publishing Ltd

Biomedical Physics & Engineering Express

Check for updates

OPEN ACCESS

RECEIVED
5 June 2025

REVISED
31 August 2025

ACCEPTED FOR PUBLICATION
17 September 2025

PUBLISHED
1 October 2025

Original content from this work may be used under the terms of the Creative Commons Attribution 4.0 licence.

Any further distribution of this work must maintain attribution to the author(s) and the title of the work, journal citation and DOI.

PAPER

Impact of metal nanoparticles on cell survival predicted by the local effect model for cells in suspension and tissue. Part 1: theoretical framework

Hans Rabus[1,*] **and Leo Thomas**[1,2]

[1] Physikalisch-Technische Bundesanstalt, Berlin, Germany
[2] Technische Universität Berlin, Berlin, Germany
[*] Author to whom any correspondence should be addressed.

E-mail: hans.rabus@ptb.de

Keywords: nanoparticle radiosensitization, local effect model, nanoparticle dose enhancement, metal nanoparticles

Supplementary material for this article is available online

Abstract

This work investigates the change in cell survival predicted by the local effect model (LEM) for an irradiated cell containing metal nanoparticles (MNPs) depending on the distribution of neighboring cells and the uptake of MNPs into the cells. In this first part of the paper, the theoretical framework is described, which is based on analytical weighting functions for the energy deposition around a single MNP and radially symmetric distributions of MNPs. The weighting functions allow calculation of the radial profile of the absorbed dose in the cell nucleus as well as the mean dose and the mean square of the dose in the nucleus. The latter two quantities determine cell survival according to the LEM. The weighting functions are applied to isolated cells in a localized MNP distribution, cells in solution, and densely packed cells in tissue. It is shown that only for the idealistic case of complete uptake of MNPs it is sufficient to consider an isolated cell, as this otherwise leads to significant underestimation in more realistic situations. In the case of cells in tissue, the MNP concentration within the range of secondary particles around the cell must be taken into account. Different packing densities of the cells may lead to values differing by up to 30% for the mean dose in the cell nucleus, depending on the conceived scenario for the uptake of MNPs. The weighting function offers a versatile method for assessing cell survival under irradiation in the presence of MNPs by the LEM, which is more general than previously reported approaches which relied on a power-law dependence of the radial dose distribution.

1. Introduction

Since Hainfeld *et al* (2004) showed in their pioneering work that the presence of gold nanoparticles (NPs) in biological cells exposed to ionizing radiation results in decreased cell survival, gold and other metal nanoparticles (MNPs) have been explored as potential agents for improving radiation therapy of cancer (Jain *et al* 2012). A roadmap for the clinical use of gold NPs as radiation sensitizers was presented by (Schuemann *et al* 2016) and challenged by (Cui *et al* 2017). The state of the art of enhancement of radiation effects by nanoparticles (including but not limited to gold) was reviewed by (Kuncic and Lacombe 2018), and the translational challenges were explored in a more generic roadmap for metal nanoparticles in radiation therapy (Schuemann *et al* 2020). The use of nanoparticles in clinical trials was recently reviewed by (Kumarasamy *et al* 2024).

Numerous Monte Carlo (MC) simulation studies have tried to explain this dose enhancement or radiosensitizing effect of MNPs as reviewed, e.g. by (Chow 2018). While the majority of studies considered pure gold nanoparticles, more advanced types of NPs such as gold-coated magnetic NPs (Xu *et al* 2022) or radioactive NPs (Kim *et al* 2024) have also been investigated.

Many simulations considered the enhanced energy deposition around a single MNP as an initial step, e.g. (McMahon *et al* 2011b, 2011a) for

© 2025 The Author(s). Published by IOP Publishing Ltd

megavoltage x-rays. (Lin *et al* 2014) presented a comparison of radiation qualities, and (Zygmanski and Sajo 2016) and (Martinov and Thomson 2017) explored the challenge of connecting simulations of macroscopic radiation transport with nanoscale details of radiation effects around MNPs. Analytical models are used to achieve the transition from the dose distribution around a single MNP to the dosimetric effects at the cellular level, e.g. in (Lin *et al* 2015).

In many of these studies, simplified concentric spherical geometries were considered such as in (Lin *et al* 2015) and (Xie *et al* 2015). Some of these studies used the local effect model (LEM) of Krämer and Scholz (2000) to predict cell survival. Examples include the work of McMahon *et al* (2011a) and Lin *et al* (2015) where details on how the corresponding integration over the three-dimensional dose distribution was achieved were not given. In their replication study of the work of Lin *et al* (2015), Velten and Tomé (2023) introduced a two-dimensional version of the LEM. Pitfalls related to simplifications for computational feasibility of application of the LEM to MNPs may lead to severe overestimation of the reduction in cell survival as pointed out in (Rabus 2024b) and later confirmed by (Velten and Tomé 2024).

Methodologically more sound approaches have been presented by Melo-Bernal *et al* (2021) and Rabus (2024b), assuming a simple power law describing the radial dose profile around an MNP. In the present work, these earlier approaches are developed and used to assess to what extent investigations considering MNPs in and around a single cell such as in (McMahon *et al* 2011a, Lin *et al* 2015, Velten and Tomé 2023) are representative of realistic scenarios of cells in suspension or densely packed in tissue.

The approaches used by Melo-Bernal *et al* (2021), Rabus (2024b) and the present work make use of the fact that absorbed dose is an expectation value. Namely, the expectation value of the distribution of the stochastic quantity specific energy (energy imparted per mass) (Braby *et al* 2023). MC simulations rely on the law of large numbers which ensures that the mean specific energy as determined by MC sampling converges to this expectation value. Therefore, the sample-mean and the sample standard deviation can be used as estimates of the absorbed dose and its uncertainty.

In the case of the strongly heterogenous geometry with MNPs in a cellular environment, MC sampling faces two critical challenges:

First, the probability of an MNP responding to the radiation, i.e., of an ionizing interaction to occur in it, is generally small. For instance, with photons from a 50 kV x-ray spectrum, the expected number of interactions in a gold NP of 50 nm diameter is 1.1×10^{-3} (Rabus *et al* 2021a) when a photons hits the NP. The probability of a photon hitting a particular NP in an MC simulation is given by the ratio of the cross-section of the NP and the cross-section of the photon beam. If the beam has a square cross section of 10 μm side (typical dimension of a mammalian cell), this probability is about 2×10^{-5}. The resulting number of ionizing interactions per primary photon is thus about 2×10^{-8}. Therefore, depending on the number of primary particles simulated only a proportion of the MNPs present undergo an ionizing interaction, and the sample-mean only refers to this subset of MNPs. However, in order to obtain an estimate of the absorbed dose, the simulations would have to be performed with a number of primary particles so large that all MNPs undergo a large number of photon interactions. Otherwise, the sampling statistics may result in outcomes that are not representative of the expectation value.

Second, and more important, a single simulation with a given distribution of MNPs is only representative of this statistical sample of MNP locations. Therefore, in practice, MC simulations do not determine an estimate of the statistical expectation value for a uniform spatial distribution but rather for a single sample drawn from such a spatial distribution. In order to exploit the law of large numbers, the MC simulations would have to be repeated several times with sufficiently large number of events and a new geometry rendering of the NP positions before each simulation run.

Both challenges impose a large number of required simulated histories that are presently difficult to realize. If the geometry rendering was done 100 times and each simulation then aimed at 100 interactions per MNP, the number of primary photons to be simulated would be 5×10^{12} for the very favorable case of gold NPs with a diameter of 50 nm and 50 kV x-rays. For an NP diameter of 5 nm, this number would be a factor of 1000 larger, and for a ^{60}Co spectrum with three orders of magnitude lower interaction probability (Rabus and Mkanda 2025), there would be another factor of 1000 more. Therefore, it appears that determining absorbed dose from a distribution of MNPs in a cell requires an approach different from direct MC simulation.

Similar to preceding work of Melo-Bernal *et al* (2021) and Rabus (2024b), the analysis is based on idealizing assumptions such as that the dose distribution around an MNP is radially symmetric and that MNPs are present in spatially uniform distributions in parts of the considered geometry. While the emission of secondary particles and the resulting spatial distribution of energy imparted may not be exactly spherically symmetric, anisotropy only occurs in the vicinity of the MNP (Derrien *et al* 2023) and, even there, the anisotropy was shown to be in the range of a few percent (Rabus 2024a). Similarly, MNPs tend to be non-uniformly distributed in and between cells, which leads to statistical variations in cell survival, as discussed by Zygmanski *et al* (2013).

This implies caveats to the present approach, which should still be sufficient for addressing questions such as whether predictions of cell survival based on simulations considering isolated cells (Lin *et al* 2015) are representative of the expected outcome for cells in suspension in radiobiological experiments or for survival of cells in tissue.

The approach used in this work is based on geometrical weighting functions for the radial distribution of energy imparted around a single spherical MNP. These weighting functions allow calculation of the radial dose profile in a spherical cell nucleus as well as of the mean dose and the variance of the dose in a spherical cell nucleus from the radial distribution of the dose around a single MNP. This approach is more general than those presented previously by Melo-Bernal *et al* (2021) and Rabus (2024b), in that no assumption is made regarding the functional dependence of the dose distribution around an MNP. The weighting functions can be applied to MNPs of any material and also to the often-considered water NP of the same size.

Such weighting functions are determined for the case of a uniform MNP distribution in a sphere surrounding the cell nucleus as well as for simple extensions such as MNPs only in a spherical shell or MPNs at different concentration in a sphere and one or two spherical shells around. The generalization to a continuously varying radially symmetric concentration profile of MNPs is also discussed. General considerations are made regarding the suitability of approaches found in the literature that consider a localized MNP distribution around a single cell. In addition, the case of cells in tissue is considered, and the applicability of a simplified surrogate model of the MNP concentration. Application of the model with dose distributions around MNPs from several recent publications will be discussed in the second part of the paper.

2. Materials and methods

2.1. The local effect model

The LEM formulated by Krämer and Scholz (2000) assumes that the survival probability of a cell exposed to an ion beam producing a largely inhomogeneous dose distribution is given by equation (1):

$$S_i(D) = e^{-N_i} \tag{1}$$

In equation (1), N_i is the expected number of lethal lesions produced in the cell nucleus, which is given by equation (2):

$$N_i(\bar{D}, \overline{D^2}; \alpha, \beta, D_t) = \langle N_u \rangle = \iiint_{V_n} \frac{N_u(D(\vec{r}); \alpha, \beta, D_t)}{V_n} dV_n \tag{2}$$

Herein, $D(\vec{r})$ is the local dose at point $\vec{r}$, V_n is the volume of the cell nucleus, and α, β, D_t are the coefficients of the linear quadratic linear (LQL) model of cell survival applying to irradiation with photons at a uniform dose distribution (over the dimensions of a cell). The expected number $N_u(D; \alpha, \beta, D_t)$ of lesions in the nucleus for a uniform dose distribution in the LQL model is given by equation (3):

$$N_u(D; \alpha, \beta, D_t) = \begin{cases} \alpha D + \beta D^2 & D \leqslant D_t \\ (\alpha + 2\beta D_t)D - \beta {D_t}^2 & D > D_t \end{cases} \tag{3}$$

In equation (3), D_t is the threshold dose for transition between the linear quadratic dose dependence to the high-dose linear dose dependence. It should be noted that the functional dependence of N_u on D is continuous and smooth at $D = D_t$.

The quantities $\bar{D}$ and $\overline{D^2}$ on the left-hand side of equation (2) are the mean dose and mean square of the dose in the nucleus, respectively (equation (4)):

$$\begin{aligned} \bar{D} &= \frac{1}{V_n}\int_{V_n} D(\vec{r})\, dV_n \\ \overline{D^2} &= \frac{1}{V_n}\int_{V_n} D^2(\vec{r})\, dV_n \end{aligned} \tag{4}$$

The quantity $N_i(\bar{D}, \overline{D^2}; \alpha, \beta, D_t)$ is thus the integral of the spatial density of the expected lesions and can be expressed by equation (5)[3]:

$$N_i(\bar{D}, \overline{D^2}; \alpha, \beta, D_t) = \alpha\bar{D} + \beta\bar{D}^2 + \beta\overline{(D - \bar{D})^2} - \beta\langle (D - D_t)^2 \rangle_t \tag{5}$$

The third term on the right-hand side of equation (5) is the variance of the dose. The quantity $<(D - D_t)^2>_t$ represents the mean squared excess dose over the regions in the cell nucleus in which the dose D exceeds D_t, as indicated by the integration domain V_t in equation (6):

$$\langle (D - D_t)^2 \rangle_t = \frac{1}{V_n}\int_{V_t} (D(\vec{r}) - D_t)^2 dV_t \tag{6}$$

The term defined by equation (6) leads to a reduction in the number of predicted lesions as per equation (5). Neglecting this term, as we also do following the example of Melo-Bernal *et al* (2021), therefore gives an upper bound for the expected number of lesions. It must be emphasized, however, that if the mean dose exceeds the threshold dose, then the volume V_t comprises the whole nucleus, and the following linear expression is obtained:

[3] By virtue of $2D_tD - {D_t}^2 = D^2 - (D - D_t)^2$.

Table 1. Summary of the scenarios considered in this study. The second and third columns specify the intracellular distribution of MNPs by giving the ratios of the nanoparticle concentrations in the nucleus ($\bar{n}_n$) and cytoplasm ($\bar{n}_p$) to the average nanoparticle concentration in a cell ($\bar{n}_c$). The fourth and fifth columns show the ratios of the MNP concentrations in cells and in the extracellular region ($\bar{n}_{xt}$) to the overall average MNP concentration ($\bar{n}_a$). c_V is the packing density of cells or the average fraction of the volume covered by cells. V_c and V_n are the volumes of the cell and nucleus, respectively, where the radii used by (Lin *et al* 2015) were applied (i.e. $R_c = 6.75\,\mu$m and $R_n = 4\,\mu$m). V_s is the volume of a sphere of radius slightly larger (100 nm) than the nucleus. V_a and V_b are the volumes of spheres with radius $R_a = 5\,\mu$m and $R_b = 6\,\mu$m, respectively.

Scenario		$\bar{n}_n/\bar{n}_c$	$\bar{n}_p/\bar{n}_c$	$\bar{n}_c/\bar{n}_a$	$\bar{n}_{xt}/\bar{n}_a$
1	cell	1	1	$c_V{}^{-1}$	0
2	nucleus	V_c/V_n	0	$c_V{}^{-1}$	0
3	cytoplasm	0	$V_c/(V_c - V_n)$	$c_V{}^{-1}$	0
4	extern	0	0	0	$(1 - c_V)^{-1}$
5	n10%	$0.1\ V_c/V_n$	$0.9V_c/(V_c - V_n)$	1	1
6	&50%	$0.1\ V_c/V_n$	$0.9V_c/(V_c - V_n)$	$(2 - c_V)^{-1}$	$2(2 - c_V)^{-1}$
7	surface	0	$V_c/(V_s - V_n)$	$c_V{}^{-1}$	0
8	endosome	0	$V_c/(V_b - V_a)$	$c_V{}^{-1}$	0

$$N_i(\bar{D}, \overline{D^2}; \alpha, \beta, D_t) = (\alpha + 2\beta D_t)\bar{D} - \beta {D_t}^2 \quad (7)$$

In this work, the quantities $\bar{D}$ and $\overline{D^2}$ entering equation (5) are derived from the radial dose distribution around a single MNP undergoing an ionizing interaction using geometrical weighting functions derived from the geometrical distribution of MNPs for different scenarios.

2.2. Scenarios of MNP distributions

Many studies in the literature on the dosimetric effects of MNPs at the cellular level have focused on a single cell only. For instance, Lin *et al* (2015) considered several cases of distributions: (1) MNPs only in the cell; (2) MNPs uniformly distributed only in the cell nucleus; (3) MNPs only in the cytoplasm; (4) MNPs only in a thin spherical shell outside the cell; and (5) MNPs uniformly distributed in the cytoplasm and in a thin spherical shell outside the cell at the same concentration and in the cell nucleus at a different concentration.

The first three correspond to extreme cases, in all of which there is a complete uptake of all available MNPs into the cell. In the secondcase, there is even complete uptake by the cell nucleus, which may be considered the ideal case for achieving optimum dose enhancement. The last case may be considered more realistic, in that the nuclear membrane may hinder diffusion of MNPs into the cell nucleus without completely suppressing it, while there is a uniform concentration outside the cell nucleus.

These cases are also among the potential scenarios for MNP uptake by cells considered in the present work (see table 1). The first five scenarios correspond to those of (Lin *et al* 2015). In scenarios 1 to 3, there is a complete uptake of the MNPs into the cells, where the MNPs have a uniform concentration throughout the cell or only in the nucleus or only in the cytoplasm. In scenario 4, there is no uptake by the cells, so that the MNPs are only outside. In scenario 5, the average concentration of MNPs in the cell is the same as outside, while only 10% of the MNPs inside the cell are within the nucleus. The additional scenario 6 assumes that the concentration of MNPs in the cell is half that outside the cell, and only 10% of the MNPs in the cell are within the nucleus. In scenario 7, the MNPs are only near the outer surface of the cell nucleus, and in scenario 8, they are only in the middle of the cytoplasm (mimicking MNPs in an endosome).

These scenarios are characterized by the expected number densities (particles per volume) of MNPs undergoing an ionizing interaction in the nucleus ($\bar{n}_n$), the cytoplasm ($\bar{n}_p$), and in the extracellular region ($\bar{n}_{xt}$). The intracellular distribution of MNPs is characterized by the ratios of $\bar{n}_n$ and $\bar{n}_p$ to the average number density of interacting MNPs in the cell ($\bar{n}_c$). These ratios are listed in the second and third columns of table 1. For the first six scenarios, these ratios depend only on the ratio of the volume of the nucleus to that of the cell. The last two columns of table 1 give the ratios of $\bar{n}_c$ and $\bar{n}_{xt}$ to the average number density ($\bar{n}_a$) of interacting MNPs in the considered geometry. This average depends parametrically on the proportion of the volume (c_V) occupied by the cell(s).

However, the assumption that MNPs are confined to a region slightly larger than the cell appears not to be very relevant. If the envisaged scenario is a solution of cells in water, as encountered in radiobiologic cell experiments, then it would be more plausible to assume the concentration outside the cell to be uniform everywhere outside cells. Another plausible assumption is then that MNPs are distributed in neighboring cells in the same way as in the considered cell. This will change the density of MNPs contributing to the dose in the considered cell, particularly if cells are densely packed within tissue.

Therefore, four different cases are considered (table 2) in this work: isolated cells with MNPs present only in their proximity; cells in solution; and surrogate models for cells in tissue represented by densely

Table 2. Summary of the cases considered in this study. The packing density given in the third column is the fraction of total volume taken by the spheres representing the cells. R_n and R_c are the radius of the nucleus and the cell, respectively. R_x is the maximum radial distance. The first case is the one considered by (Lin *et al* 2015). The cases sFCC and sSC are the surrogates for densely packed cells in a face-centered cubic (FCC) and simple cubic (SC) lattice in which the MNP concentration outside a considered cell is replaced by the corresponding average concentration.

Case number and name		Packing density c_V	R_x/R_n	$\bar{n}_x$
1	isolated	$\frac{{R_n}^3}{(2R_c-R_n)^3}$	$2\frac{R_c}{R_n}-1$	$\bar{n}_{xt}$
2	solution	10^{-3}	30	$n_c c_V + \bar{n}_{xt}(1-c_V)$
3	sFCC	$\frac{\pi}{3\sqrt{2}}$	30	$n_c c_V + \bar{n}_{xt}(1-c_V)$
4	sSC	$\frac{\pi}{6}$	30	$n_c c_V + \bar{n}_{xt}(1-c_V)$

packed spheres in simple cubic (SC) and face-centered cubic (FCC) lattices. (An FCC lattice has the highest packing density among cubic lattices). The packing densities are given in the second column of table 2 The other two columns give the ratio of an effective outer radius R_x of a spherical MNP distribution to that of the nucleus (R_n) and the effective number density $\bar{n}_x$ of interacting MNPs outside the cell.

For the case of an isolated cell, the MNPs in scenarios 1 and 2 are uniformly distributed in a single sphere that is concentric to the spherical nucleus. The corresponding geometric weighting functions are derived in section 2.3. In scenarios 3, 4, 6, and 7, the MNPs are uniformly distributed in a single spherical shell that is concentric with the nucleus. The derivation of the corresponding weighting functions is given in appendix A3. Scenarios 5 and 6 consider MNPs at different concentrations in a sphere and two concentric spherical shells. The corresponding weighting function is described in section 2.4 (and derived in appendix A5).

For the other cases, the MNP distribution around a particular nucleus is no longer spherically symmetric. Since the dose contributions depend only on the radial distance to the MNP, only the average number density of MNPs at a given distance is relevant. This number density is generally a complicated function of the radial distance, and the corresponding weighting functions are derived in appendices A6 and A7. In this work, it is also investigated how well the more complex radial MNP distribution and the related weighting functions can be approximated by a surrogate model similar to scenario 6, i.e., an MNP distribution that has constant values in the nucleus, the cytoplasm, and the extracellular region. This effective extracellular distribution is characterized by two parameters, an effective outer radius R_x and an effective number density $\bar{n}_x$ of emitting MNPs, that are listed in the last two columns of table 2.

2.3. Weighting functions for dosimetric effects in a spherical cell nucleus from a uniform distribution of MNPs inside a concentric sphere

In the following it is assumed that the nucleus is a sphere of radius R_n and that N_m MNPs made of material m are uniformly distributed in a concentric sphere of radius $R_c \geqslant R_n$. If p_m is the expected number of ionizing radiation interactions in an MNP (or decays for radioactive MNPs), then the expected number of MNPs emitting electrons or photons is given by $N = N_m p_m$, and the number density $\bar{n}_m$ of emitting MNPs is given by equation (8):

$$\bar{n}_m = \frac{3N_m p_m}{4\pi {R_c}^3} \tag{8}$$

For a given geometrical arrangement of the N emitting MNPs at positions $\vec{r}_i$ ($i = 1, 2, \ldots, N$), the absorbed dose at a point $\vec{r}$ in the nucleus is given by equation (9):

$$D(\vec{r}) = D_w + \sum_{i=1}^{N} D_1(|\vec{r} - \vec{r}_i|) \tag{9}$$

Here, D_w is the dose contribution originating in interactions of the incident radiation occurring outside MNPs (zero for radioactive MNPs). The contribution from one emitting MNP, D_1, is the expected energy imparted per mass at a given radial distance from the center of the MNP due to the particles emitted from the MNP after ionizing radiation interaction or a decay event.

The mean value of the dose and the square of the dose in the nucleus for a fixed geometrical arrangement of the N emitting MNPs are given by equations (10) and (11), respectively:

$$\bar{D} = \frac{1}{V_n}\int_{V_n} D(\vec{r})dV = D_w + \frac{1}{V_n}\int_{V_n}\sum_{i=1}^{N} D_1(|\vec{r} - \vec{r}_i|)dV_n \equiv D_w + \bar{D_N} \tag{10}$$

$$\overline{D^2} = {D_w}^2 + 2D_w\overline{D_N} + \overline{D_{Ns}^2} + \overline{D_{Np}^2} \tag{11}$$

The quantities $\overline{D_{Ns}^2}$ and $\overline{D_{Np}^2}$ are the contributions of all individual MNPs and of all pairs of MNPs to the mean square of the dose given by equations (12) and (13):[4]

$$\overline{D_{Ns}^2} = \frac{1}{V_n}\int_{V_n}\sum_{i=1}^{N}[D_1(|\vec{r} - \vec{r}_i|)]^2 dV_n \tag{12}$$

[4] A list of frequently used symbols and their explanations can be found in Supplementary table 1.

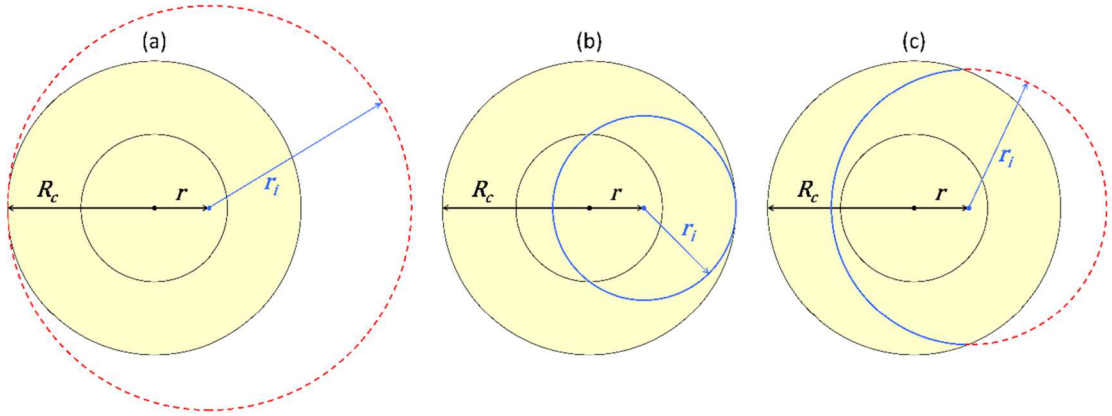


Figure 1. Schematic illustration of geometrical weighting. In each graph, the yellow shaded circle represents a cut through the sphere containing nanoparticles by a plane passing through its center and a point at a radial distance r. The small black circle represents the cell nucleus. The blue circle and blue arc indicate the part of a sphere surface around the chosen point inside the sphere containing nanoparticles, the red dashed arc and circle indicate the portion of the sphere surface outside the region with nanoparticles. (a) corresponds to the first case in equation (17), namely distances r_i to the MNP of at least the sum of the radius R_c of the spherical region containing MNPs and the radial distance r of the considered point (at which the dose is determined) from the center of the nucleus. In this case there are no MNPs located at a distance r_i from the considered point. (b) corresponds to the second case in equation (17), that is, distances r_i to the MNP not greater than the difference between R_c and r. In this case MNPs located at a distance r_i from the considered point cover the whole solid angle. (c) corresponds to the third case in equation (17), that is, distances r_i for which MNPs are found on a part of the solid angle on a sphere of radius r_i around the considered point.

$$\overline{D_{Np}^2} = \frac{1}{V_n}\int_{V_n}\sum_{i=1}^{N}\sum_{j\neq i} D_1(|\vec{r}-\vec{r}_i|)D_1(|\vec{r}-\vec{r}_j|)dV_n \tag{13}$$

These two quantities determine the variance of the dose, as shown in equation (14):

$$\mathrm{Var}(D) \equiv \overline{(D-\bar{D})^2} = \overline{D_{Ns}^2} + \overline{D_{Np}^2} - \overline{D_N}^2 \tag{14}$$

2.3.1. Weighting function for the dose at a point in the cell nucleus

Equation (9) makes use of the fact that the absorbed dose is an expectation value and gives the absorbed dose conditional on the geometrical arrangement of the N emitting MNPs. To obtain the unconditional expectation value representing the absorbed dose for a uniform distribution of MNPs in a sphere, equation (9) must be averaged over all possible arrangements of the N emitting MNPs. This can be achieved by replacing the sum by an integral over the probability density of MNP positions, which is constant and given by equation (8). This leads to equation (15):

$$D(\vec{r}) = D_w + \int_{V_c} \bar{n}_m \times D_1(|\vec{r}-\vec{r}_i|)dV_c \tag{15}$$

It should be noted that by the definition of absorbed dose, in both equations (9) and (15), $D(\vec{r})$ is an expectation—in the former case for a fixed arrangement of the MNPs, and in the latter case for a uniform distribution of emitting MNPs in a volume. This means that equation (15) corresponds to the statistical average over all possible geometrical arrangements compatible with the requirement that the MNP distribution is to be spatially uniform. In contrast to the results from an MC simulation which provides an estimate for the absorbed dose for a given geometrical arrangement of MNPs, the dose calculated according to equation (15) corresponds to an expectation-true estimator of the dose from a uniform distribution of MNPs.

To evaluate the integral on the right-hand side, it is advantageous to choose the point $\vec{r}$ as the center of the coordinate system (blue point in figure 1) and introduce spherical coordinates. This transforms equation (15) into equation (16):

$$D(\vec{r}) = D_w + \bar{n}_m \int_{r_p}^{\infty} D_1(r_i)\Omega(r_i, r|R_c)\,{r_i}^2 dr_i \tag{16}$$

In equation (16), r_p denotes the radius of the spherical MNP, and ${r_i}^2\Omega(r_i, r|R_c)$ is the part of the surface of a sphere of radius r_i around a point at distance r from the center of the nucleus which falls inside the sphere where MNPs are present. In figure 1, this region is indicated by the yellow shaded area, and a portion of the surface inside the sphere containing the MNPs is indicated by the blue circle and arc, respectively. The solid angle subtended by the part of the surface inside the region with MNPs is given by equation (17), where the three cases correspond to the situations illustrated in figures 1(a)–(c):

$$\Omega(r_i, r|R_c) = \begin{cases} 0 & r < r_i - R_c \\ 4\pi & r < R_c - r_i \\ \pi\dfrac{{R_c}^2 - (r-r_i)^2}{r_i r} & \text{else} \end{cases} \tag{17}$$

The first of the three cases in equation (17) means that the distance r_i from the considered point is so large that all points at this distance from a point inside

the nucleus are outside the region containing MNPs. The red dashed circle in figure 1(a) corresponds to the smallest value of r_i for which this is the case. The second case in equation (17) applies to all points in the nucleus for which the whole sphere of radius r_i is within the region containing MNPs. The solid blue circle in figure 1(b) indicates the largest sphere for which this applies. The third case corresponds to distances r_i from the chosen point for which some points are inside (blue arc in figure 1(c)) and some are outside (red dashed arc in figure 1(c)).

2.3.2. Mean dose in a cell nucleus from a uniform distribution of MNPs inside a sphere

As shown in section S1.1 of Supplement 1, the average excess dose $\overline{D_N}$ produced in a spherical nucleus (radius R_n) from a uniform distribution of MNPs in a concentric spherical volume (radius R_c, volume V_c) can be written as follows:

$$\overline{D_N} = \bar{n}_m \overline{d_1}(R_c) \tag{18}$$

In equation (18), $\bar{n}_m$ is the number density of emitting MNPs in the volume V_c, and $\overline{d_1}$ is the ratio of the dose contribution from a single emitting MNP to the number density of one emitting MNP in V_c and can be obtained from the radial dose distribution around an emitting nanoparticle by the following relation:

$$\overline{d_1}(R_c) = \int_{r_p}^{\infty} D_1(r_i) {r_i}^2 \times 4\pi \bar{\omega}(r_i|R_c)\, dr_i \tag{19}$$

The dimension of $\overline{d_1}$ is dose times volume. The symbol r_i in equation (19) denotes the radial distance from the nanoparticle, and $\bar{\omega}(r_i|R_c)$ is a weighting function defined by equation (20):

$$\bar{\omega}(r_i|R_c) = \frac{3}{{R_n}^3} \int_0^{R_n} \frac{\Omega(r_i,\, r|R_c)}{4\pi} r^2 dr \tag{20}$$

Explicit expressions for the weighting function are given in appendix A1. The quantity $\bar{\omega}(r_i|R_c)$ is the mean fraction of the surface area of a sphere of radius r_i around an arbitrary point within the nucleus that is within the region loaded with MNPs, averaged over the cell nucleus.

2.3.3. Mean square of the dose in a spherical cell nucleus from a uniform distribution of MNPs inside a concentric sphere

It is evident that the third term in equation (11) can be treated in the same way as $\overline{D_N}$. This leads to equation (21) for the contribution $\overline{D_{Ns}^2}$ to the square of the dose from the dose around individual MNPs:

$$\overline{D_{Ns}^2} = N\overline{D_1^2} = \bar{n}_m \overline{d_1^2} \tag{21}$$

In equation (21), $\overline{D_1^2}$ is the average contribution to the mean square of the dose in the nucleus from a single emitting MNP, and $\overline{d_1^2}$ is the corresponding average contribution per number density of emitting MNPs given by equation (22):

$$\overline{d_1^2}(R_c) = \int_{r_p}^{\infty} [D_1(r_i)]^2 r_i^2 \times 4\pi \bar{\omega}(r_i|R_c)\, dr_i \tag{22}$$

The last term in equation (11) can be written in an analogous way (see Supplement 1, section S1.3). This gives the following expression for the contribution $\overline{D_{Np}^2}$ to the mean square of the dose in the nucleus from all pairs of MNPs undergoing an ionization, where V_p denotes the volume of the MNP:

$$\overline{D_{Np}^2} = {\bar{n}_m}^2 \times [\overline{d_2^2} - 8V_p \times \overline{d_1^2}] \tag{23}$$

The quantity $\overline{d_2^2}$ (equation (24)) is the ratio of the average synergistic contribution from a pair of MNPs to the square of the number density of emitting MNPs:

$$\overline{d_2^2}(R_c) = \int_{r_p}^{\infty} \int_{r_p}^{\infty} D_1(r_i) {r_i}^2 D_1(r_j) {r_j}^2 \times (4\pi)^2 \bar{\omega}_2(r_i,\, r_j|R_c)\, dr_j\, dr_i \tag{24}$$

In equation (24), $\bar{\omega}_2(r_i,\, r_j|R_c)$ is a bivariate weighting function defined by equation (25):

$$\bar{\omega}_2(r_i,\, r_j|R_c) = \frac{3}{{R_n}^3} \int_0^{R_n} \frac{\Omega(r_i,\, r|R_c)}{4\pi} \frac{\Omega(r_j,\, r|R_c)}{4\pi} r^2 dr \tag{25}$$

Explicit expressions for the function $\bar{\omega}_2(r_i,\, r_j|R_c)$ are given in appendix A2.

2.3.4. Weighting function for the variance

From equations (14), (21), and (23), the variance Var(D) of the dose can be written as

$$\begin{aligned} \mathrm{Var}(D) &= \bar{n}_m \bar{d_1^2}(1 - \bar{n}_m 8V_p) + {\bar{n}_m}^2(\bar{d_2^2} - {\bar{d}_1}^2) \\ &= \bar{n}_m \times \mathrm{var}_1 + {\bar{n}_m}^2 \times (\mathrm{var}_2 - 8V_p \mathrm{var}_1) \end{aligned} \tag{26}$$

where V_p denotes the volume of the MNP. That is, the variance has one term proportional to the number density of emitting MNPs and one term proportional to the square of the number density. The quantity var_2 in the proportionality factor in this second term is given by equation (27):

$$\begin{aligned} \mathrm{var}_2 &= \overline{d_2^2} - \overline{d_1}^2 = \int_{r_p}^{\infty} \int_{r_p}^{\infty} D_1(r_i) {r_i}^2 D_1(r_j) {r_j}^2 \\ &\quad \times (4\pi)^2 \bar{\nu}_2(r_i,\, r_j|R_c)\, dr_j\, dr_i \end{aligned} \tag{27}$$

The modified weighting function appearing in equation (27) is given in equation (28):

$$\bar{\nu}_2(r_i,\, r_j|R_c) = \bar{\omega}_2(r_i,\, r_j|R_c) - \bar{\omega}(r_i|R_c)\bar{\omega}(r_j|R_c) \tag{28}$$

The quantity var_2 and the resulting contribution to the second term in equation (26) describe the contribution to the variance of the dose resulting from pairs of emitting MNPs.

2.4. Weighting functions for a spherical shell and combinations of sphere and spherical shells

The weighting functions presented in the previous section are for a uniform distribution of MNPs in a

sphere. In potential radiotherapy applications, enhanced uptake of MNPs into cells or even the cell nucleus is desirable. Adversely, the membranes of the cell or nucleus may hinder diffusion of MNPs into the cell nucleus or the cell without completely suppressing it. In both cases, the result may be that the MNPs have different number densities in the nucleus (n^-_n), the cytoplasm ($\bar{n}_p$), and the extracellular region ($\bar{n}_x$), while still being uniformly distributed in each of these regions. Examples considered in literature are situations in which the MNPs are only present in the cytoplasm or only outside the cell (Lin *et al* 2015).

Appendices A3–A5 show the derivation of the corresponding relations for the cases of MNPs only in a spherical shell, for MNPs at different concentrations in a sphere and a surrounding spherical shell, and for three different MNP concentrations in a sphere and two enclosing spherical shells. The latter case is suggested as a surrogate for the general case of a continuously varying radially symmetric concentration of emitting MNPs, for which the corresponding expressions can be found in appendices A6 and A7.

As can be seen in the appendices, the resulting contributions from single MNPs or pairs of MNPs turn out to be linear or bilinear combinations of the quantities $\overline{d_1}$, $\overline{d_1^2}$, and $\overline{d_2^2}$ described by equations (19), (22), and (24), respectively. In the case of different MNP concentrations in three radial intervals (appendix A5), the mean contribution to the dose ($\overline{D_N}$) and the square of the dose from single MNPs ($\overline{D_{Ns}^2}$) and pairs of MNPs ($\overline{D_{Np}^2}$) turn out to be given by equation (29):

$$\begin{aligned}\overline{D_N} &= \bar{n}_a \times \bar{d}_1(\theta)\\ \overline{D_{Ns}^2} &= \bar{n}_a \times \bar{d}_1^2(\theta)\\ \overline{D_{Np}^2} &= \bar{n}_a{}^2 \times (\bar{d}_2^2(\theta) - 8V_p\bar{d}_{1b}^2(\theta))\end{aligned} \tag{29}$$

Here, V_p is the volume of the MNP, and $\theta = \{R_n, R_c, R_x, u_n, u_p, u_x\}$ is the set of radii and concentrations relative to the average number density $\bar{n}_a$ in the sphere of radius R_x. $\bar{n}_a$ is related to the average number of emitting MNPs per cell, i.e., the ratio of the number density of emitting MNPs and the number density of cells present in the sphere of radius R_x, where R_x can be chosen arbitrarily large.

The quantities $\overline{d_1}(\theta)$, $\overline{d_1^2}(\theta)$, $\overline{d_2^2}(\theta)$, and $\overline{d_{1b}^2}(\theta)$ are obtained from the radial dose distribution around a single emitting MNP using equations (30)–(33), with the weighting functions w_1, w_2, and w_{1b} (explicit expressions are given in appendix A5 by equations (A19)–(A21)), respectively:

$$\overline{d_1}(\theta) = \int_{r_p}^{\infty} D_1(r_i)\, r_i{}^2 \times 4\pi w_1(r_i|\theta)\, dr_i \tag{30}$$

$$\overline{d_1^2}(\theta) = \int_{r_p}^{\infty} [D_1(r_i)]^2 r_i{}^2 \times 4\pi w_1(r_i|\theta)\, dr_i \tag{31}$$

$$\overline{d_2^2}(\theta) = \int_{r_p}^{\infty}\int_{r_p}^{\infty} D_1(r_i) r_i{}^2 D_1(r_j) r_j{}^2 \times (4\pi)^2 w_2(r_i, r_j|\theta)\, dr_j\, dr_i \tag{32}$$

$$\overline{d_{1b}^2}(\theta) = \int_{r_p}^{\infty} [D_1(r_i)]^2 r_i{}^2 \times (4\pi)^2 w_{1b}(r_i|\theta)\, dr_i \tag{33}$$

As before, $\overline{d_1}(\theta)$ is the mean contributions per average number density of emitting single MNPs to the mean dose in the nucleus. Correspondingly, $\overline{d_1^2}(\theta)$ is the mean contributions per average number density of emitting MNPs to the mean square of the dose in the nucleus due to single MNPs. The quantity $\overline{d_2^2}(\theta) - 8V_p\overline{d_{1b}^2}(\theta)$ is the mean contribution to the square of the dose in the nucleus from pairs of MNPs normalized to the square of the average number density of MNPs. The first term of this difference is what one gets by ignoring the fact that the two different MNPs must be at distinct locations (i.e. have a distance of at least the diameter of an MNP). The second term is the corresponding approximate correction for non-overlap between MNP.

2.5. Application of the weighting functions

The radial dose distribution around an MNP is obtained, e.g. by MC simulation, as an average dose in a spherical shell. This yields an estimate of the function $D_1(r_i)$ by a piecewise constant function. Evaluation of equations (30)–(33) then gives equations (34)–(37)

$$\overline{d_1}(\theta) = \sum_{k=1}^{k_{\max}} \overline{D_1}(r_k)\, r_k{}^2 \times 4\pi w_1(r_k|\theta)\, \Delta r_k \tag{34}$$

$$\overline{d_1^2}(\theta) = \sum_{k=1}^{k_{\max}} [\overline{D_1}(r_k)]^2 r_k{}^2 \times 4\pi w_1(r_k|\theta)\, \Delta r_k \tag{35}$$

$$\overline{d_2^2}(\theta) = \sum_{k=1}^{k_{\max}}\sum_{n=1}^{n_{\max}} \overline{D_1}(r_k) r_k{}^2 \overline{D_1}(r_n) r_n{}^2 \times (4\pi)^2 w_2(r_k, r_n|\theta)\, \Delta r_k\, \Delta r_n \tag{36}$$

$$\overline{d_{1b}^2}(\theta) = \sum_{k=1}^{k_{\max}} [\overline{D_1}(r_k)]^2 r_k{}^2 \times 4\pi w_{1b}(r_k|\theta)\, \Delta r_k \tag{37}$$

Here, r_k and r_n are the mean radius of the k-th and n-th radial shell, respectively, $\overline{D_1}(r_k)$ and $\overline{D_1}(r_n)$ are the corresponding mean dose values, and Δr_k and Δr_n are the corresponding shell thicknesses. Equations (34)–(37) are approximate and apply to the case that the thickness of the radial shells is small. If this is not the case, then interpolations of the radial dose distributions must be applied. In the numerical evaluations of this work, the quantity $\overline{D_1}(r_k) \times r_k{}^2$ (proportional to the dose-area-product) is interpolated using cubic-spline interpolation. Given the peak-like structures that may be present in the dose-area-product from the Bragg peaks of Auger electrons (see, e.g., Supplementary figure 6), this local approximation appears beneficial over attempts at approximating the complete radial dose dependence in closed form by a simple analytical function.

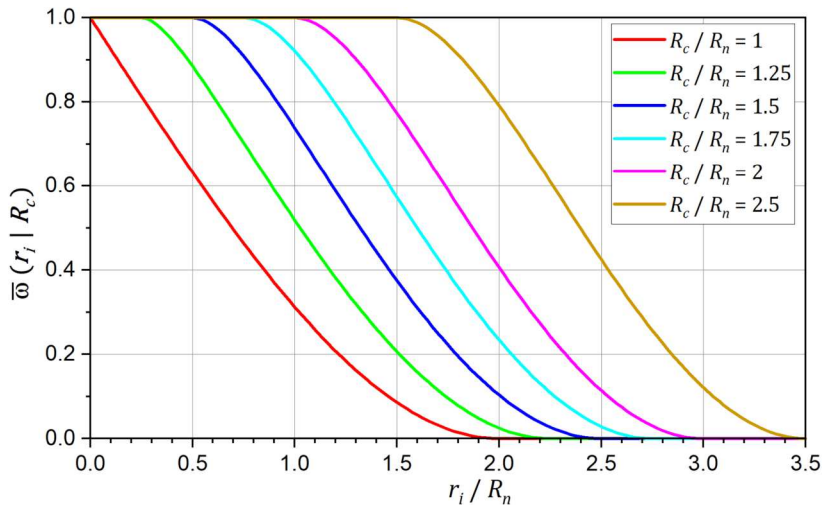


Figure 2. Weighting function for calculating the mean contribution per emitting MNP to the dose in the cell nucleus (radius R_n) from the radial dose distribution around a single MNP. The MNPs are uniformly distributed in a sphere of radius R_c which is concentric to the nucleus. The different curves correspond to different ratios of R_c/R_n (see legend). (R_n is the radius of the nucleus, R_c is the radius of the sphere containing MNPs, and r_i is the considered radial distance between a given point and an MNP.

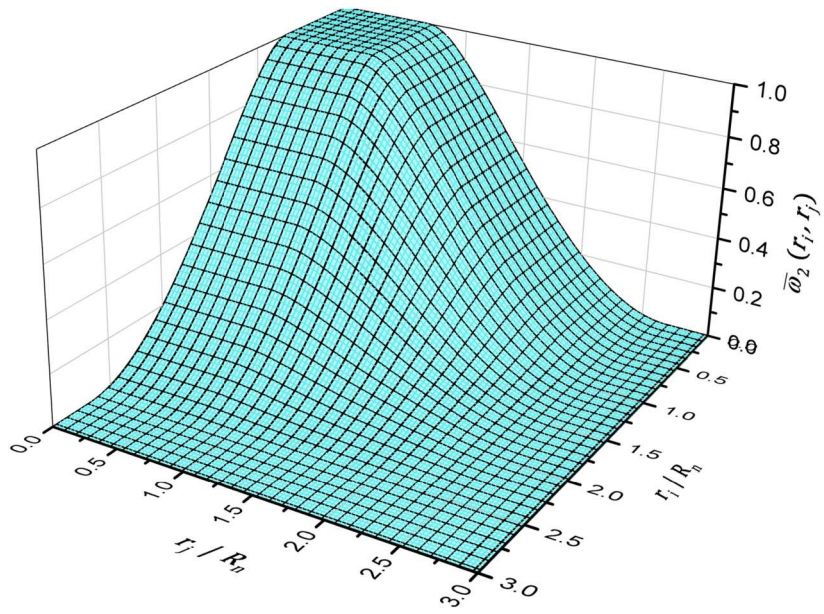


Figure 3. Functional dependence of the weighting function $\bar{\omega}_2$ (see equation (25) and appendix A2) for pairs of MNPs (contributing to the mean square of the dose in the nucleus) on the ratios r_i/R_n and r_j/R_n (x- and y-axes) for the value a = 1.6875 of the ratio R_c/R_n. (R_n is the radius of the nucleus, R_c is the radius of the sphere containing MNPs, and r_i and r_j are the considered radial distances between a given point and two MNPs).

3. Results

3.1. Elementary weighting functions for MNPs uniformly distributed in a sphere

Sample weighting functions that allow calculation of the dose in a cell nucleus for different radial distances from the nucleus center from the dose around a single MNP emitting photons or electrons can be seen in Supplementary figure 1. The curves were calculated with equation (17) for a ratio of the radius R_c of the sphere containing MNPs to that of the cell nucleus (R_n) corresponding to the cell geometry considered by (Lin *et al* 2015).

Weighting functions for calculating the mean dose to the cell nucleus for different sizes of the sphere filled with MNPs are shown in figure 2. The weighting functions were calculated according to equation (20) (explicit expressions are given in equation (A1)) for different ratios R_c /R_n between 1 (MNPs only in the cell nucleus) and 2. It can be seen in figure 2 that the weighting function peaks at radial distance 0 and monotonously decreases when the MNPs are only in

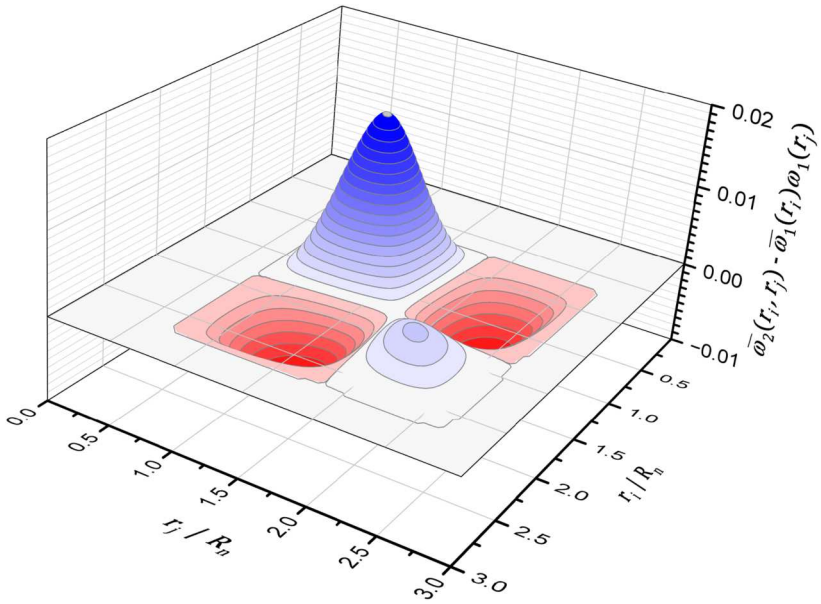


Figure 4. Functional dependence of the weighting function $\bar{v}_2$ (equation (28)) for the variance of the absorbed dose in the nucleus on the ratios r_i/R_n and r_j/R_n (x- and y-axes) for the value a = 1.6875 of the ratio R_c/R_n. (R_n is the radius of the nucleus, R_c is the radius of the sphere containing MNPs, and r_i and r_j are the considered radial distances between a given point and two MNPs.

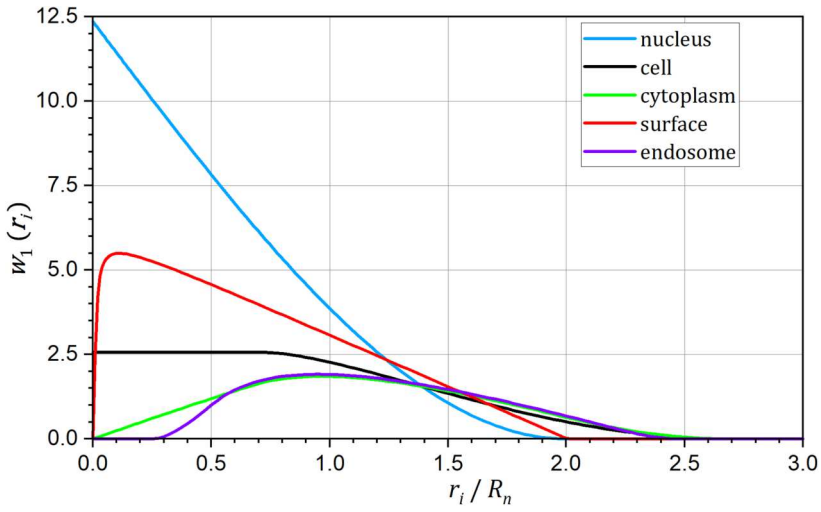


Figure 5. Weighting function for calculating the mean contribution per emitting MNP to the dose in the spherical cell nucleus (radius R_n) from the radial dose distribution around a single MNP (which depends on r_i, the radial distance from the MNP). The different curves apply to an isolated cell and different distributions of the MNPs in different compartments of the cell (see legend). The cases are as follows: all MNPs in the nucleus; all in the cell (sphere of radius R_c); all in the cytoplasm (spherical shell of inner radius R_n and outer radius R_c); all at the nucleus surface (spherical shell of inner radius R_n and outer radius R_n+50 nm); and all in a spherical layer in the middle of the cytoplasm (spherical shell of inner radius $1.25R_n$ and outer radius $1.5R_n$) corresponding to MNPs in an endosome.

the cell nucleus. When the radius of the sphere containing MNPs exceeds the radius of the nucleus, an initial plateau is found before the function begins to fall to zero.

An example of a bivariate weighting function (determining the synergistic contribution of pairs of MNPs to the mean square of the dose) is shown in figure 3. The value of the parameter $a = R_c/R_n$ determining the distribution corresponds to the cell model used by (Lin *et al* 2015) and the case that the MNPs are uniformly distributed within the whole cell. In this case, the weighting function is unity for radial distances of up to 75% of the nucleus radius and gradually drops to zero while one or both radial distances increase. Weighting functions for some other choices of R_c/R_n can be found in section S1.3.1. of Supplement 1.

The functional dependence of the weighting function for the part of the variance depending quadratically on the MNP concentration can be seen in

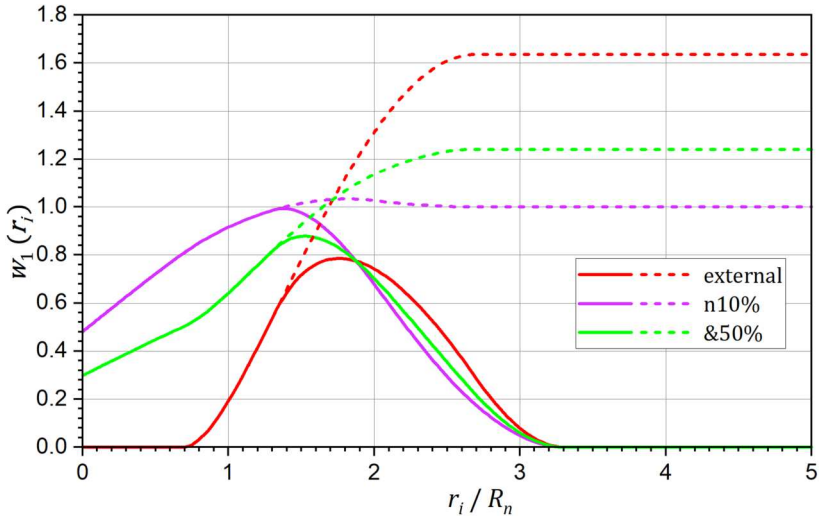


Figure 6. Weighting function for calculating the mean contribution per emitting MNP to the dose in the spherical cell nucleus (radius R_n) from the radial dose distribution around a single MNP (which depends on r_i, the radial distance from the MNP). The solid lines correspond to an isolated cell in which MNPs are contained in a sphere of radius 2.5 μm larger than the cell, as in (Lin *et al* 2015). The dashed lines correspond to cells in solution with the same concentration in the extracellular medium as for the solid lines. The cases considered are as follows: MNPs only outside the cells (red); same average concentration of MNPs in the cells as in the extracellular medium, but only 10% of the MNPs internalized in cells are inside the nucleus (magenta); the concentration in the extracellular medium is twice the average concentration inside the cells, and again 10% of the internalized MNPs are in the nucleus (green).

figure 4. A general feature of this weighting function is that it vanishes for small values of r_i/R_n and r_j/R_n, where a plateau can be seen in figure 3. It is worth noting that the peaks and troughs seen in figure 4 have only small amplitudes in the order of magnitude of 0.01. This implies that the corresponding contribution to the variance of the dose in the nucleus will only become significant at high number densities of emitting MNPs.

3.2. Isolated cells versus cells in solution

Five of the MNP uptake scenarios listed in table 1 (see Supplementary figure 2) assume a complete uptake of the MNPs by cells. Scenarios 1 to 3 correspond to cases considered by (Lin *et al* 2015) of MNPs uniformly distributed within the entire cell, only in the cell nucleus, or only in the cytoplasm. The other two cases correspond to scenarios discussed in the literature (Douglass *et al* 2012), in which MNPs aggregate at the membrane of the cell nucleus or are clustered in a region of the cytoplasm such as an endosome.

The weighting functions for the radial dose distribution around a single MNP used to calculate the mean contribution to the dose in the spherical cell nucleus per emitting MNP shown in figure 5 correspond to these scenarios. They apply to an isolated cell with a ratio R_c/R_n of the cell model used in the work of (Lin *et al* 2015) (about 1.69) with the reference concentration of MNPs pertaining to a sphere of 2.5 μm larger radius than the cell as considered in these papers. The black curve in figure 5 corresponds to MNPs uniformly distributed within the whole cell (scenario 1), whereas the blue curve is for all MNPs in the cell nucleus (scenario 2). The green line in figure 5 corresponds to scenario 3, in which the MNPs are distributed only in a spherical shell of inner radius R_b in equation (A9) identical to the radius R_n of the cell nucleus. The outer radius R_c is equal to the radius of the cell, so that MNPs are only in the cytoplasm. This weighting function prefers the dose distribution around an MNP at distances between R_n and 1.5 R_n.

It can be seen from figure 5 that the weighting function favors the dose distribution at small radii when the MNPs are only in the nucleus, where the high absolute values of the weights are related to the enhanced concentration of MNPs in the nucleus (for scenario 2). Not surprisingly, the case of the MNPs concentrated on the outer side of the nuclear membrane (red line) gives lower weights to very small radial distances which are still significantly higher than what is obtained when the MNPs are uniformly distributed within the entire cell. When the MNPs are uniformly distributed in the cytoplasm or in a layer in the middle of the cytoplasm, the curves show a peak around distances equal to the nuclear radius. Whether the MNPs are spread over the whole cytoplasm (green curve) or are only in a part that does not neighbor the nucleus (violet line) does not seem to have a big influence.

It can be seen from table 1 that the relative concentrations of MNPs listed in the fifth column depend on the fraction of the total volume that is filled by cells. For the geometry considered in the work of (Lin *et al* 2015), the fraction of the total volume is about 40%. However, if such a cell is conceived as being in a solution of cells, a volume fraction of cells of 10^{-3} is assumed in the second row of table 2. For the cell dimensions considered by (Lin *et al* 2015), this

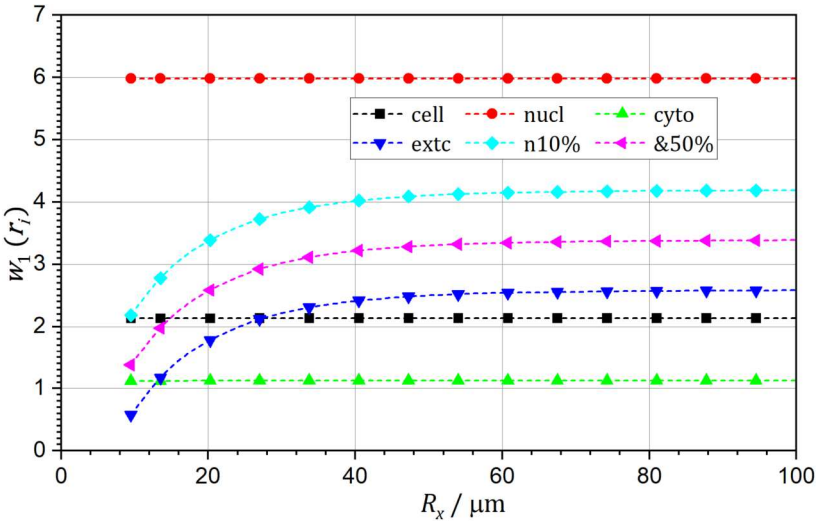


Figure 7. Dependence of the dose contribution per density of emitting MNPs on the maximum radius R_x considered in its calculation for the first six scenarios (table 1) of MNP distribution in cells in solution. The curves were produced from the data for a 50 nm gold MNP irradiated at 100 μm depth in water by a mixed photon and electron fluence spectrum originating from a 100 kVp x-ray spectrum. These data were produced with the simulation described in (Thomas *et al* 2024) scoring to distances up to 100 μm from the gold nanoparticle.

corresponds to a number density of cells in the order of 1000 μl^{-1}, which appears to be a reasonable value. For complete uptake of the MNPs into cells, this implies that the ratio of the MNP concentration in the cells to the average concentration is 1000. Using the average concentration of MNPs in the considered solution may then not be the best option. Using the concentration of MNPs internalized in cells may be preferable in such a situation, as this is also the quantity determined by experimental techniques such as atomic emission spectroscopy (Coulter 2012).

When the cells are in solution, the weighting functions for scanarios with complete uptake of the MNPs are essentially unchanged, except for a small contribution due to other cells in the order of 10^{-3}, which would not be discernible in figure 5. For the other scenarios, this is different, as illustrated in figure 6. Here, the solid lines represent the case of an isolated cell with the considered MNPs present only within a sphere about 40% larger in diameter than the cell. When the MNPs are only outside the cell (red curve), it is the dose around MNPs at distances between one and three times the nuclear radius that contributes to the dose in the nucleus. The magenta curve corresponds to the 'mixed case' of (Lin *et al* 2015) with the same average concentration in the cell and its environment but only 10% of the intra-cellular MNPs internalized in the nucleus. The solid green curve represents scenario 6 (&50%) in table 1, in which the average concentration in the cell is smaller by a factor of 2 than in the extracellular medium. In both scenarios, the presence of MNPs in the cytoplasm and nucleus results in an increased weighting of the dose distribution at small values, as could be expected.

When the cell is in solution, the assumption that the MNPs are only present in its vicinity is implausible. In this case, it appears more reasonable to assume a constant concentration of MNPs outside cells. The resulting weighting functions for the three scenarios are shown as dashed lines in figure 6. For scenario 5 (n10%, magenta), where the average concentration in the cell was assumed to be the same as outside, the weighting function essentially stays at unity instead of dropping to zero. For the other two cases, a similar plateau is obtained but with a value higher than unity. This is related to the fact that if the concentration outside cells is assumed to be constant and the average concentration is lower inside cells, then the average concentration is higher for cells in solution than for the isolated cell.

The resulting plateaus extend to infinity. This means that the complete dose profile around an MNP contributes equally to the dose in the nucleus for these uptake scenarios and cells in solution. The resulting average dose in the nucleus will thus be significantly higher than what is obtained for a single isolated cell. This is illustrated in figure 7, which shows how the estimated dose contribution per density of emitting MNPs varies with the outer radius of the region around the MNP considered in evaluating the weighting function w_1 in equation (A19).

In the scenarios with complete uptake of MNPs into the cells, there is only a small indiscernible increase in the dose contribution per MNP density. In the scenario with all MNPs outside cells (dark blue data in figure 7), there is an increase by a factor of almost 5 compared to the starting value at a radius corresponding to the region containing MNPs in the isolated cell case. When the MNP concentration outside cells is the same as the average concentration in cells (magenta symbols), the increase amounts to a factor of 2. When the concentration outside is twice the average concentration in cells, the increase is by

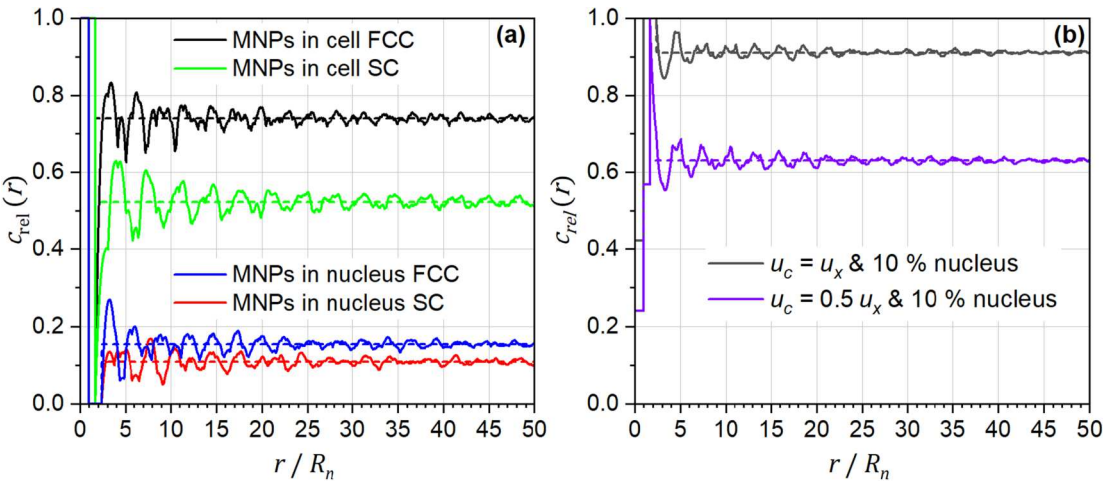


Figure 8. Average concentrations of nanoparticles at a radial distance r from the center of the nucleus (radius R_n) around a cell in tissue for (a) complete and (b) partial uptake of the MNPs by the cells. Further assumptions in (a) are a uniform distribution within the entire cell (black and green) or only in the cell nucleus (blue and red curves). The black and blue curves correspond to cells densely packed in a face-centered cubic (FCC) three-dimensional lattice, and the green and red curves to a simple cubic arrangement. In (b) the scenarios 5 and 6 from table 1 are considered, where only 10% of the MNPs in a cell are in the nucleus. The black line corresponds to equal average concentration inside and outside cells, the blue line to an average cellular concentration of 50% of the concentration in the extracellular region. The dashed lines represent the surrogate density distribution of constant value equal to the average number density at radial distances exceeding the cell radius or twice the cell's radius minus the nuclear radius (for MNPs only in the nuclei). The data correspond to the cell geometry considered by Lin *et al* (2015) and are normalized to the concentration in (a) the cell nucleus and (b) the extracellular region. Note that at small radii in (a), the red line is hidden by the blue line and the black line by the green one. In (b) the dashed blue line at small radii is hidden by the solid blue line and the dashed black and solid blue lines are hidden by the solid black line.

more than a factor of 3. This shows that with these uptake scenarios, the dose in the cell nucleus is heavily underestimated when isolated cells are considered.

3.3. Cells in tissue

If the cell is part of a tissue, it appears reasonable to assume that neighboring cells also contain MNPs at the same concentrations. (This was also implicitly assumed in the preceding for cells in solution.) For simplicity, two different regular arrangements of the cells are considered, which correspond to different packing densities. Both arrangements correspond to a cubic Bravais lattice. The less densely packed version is the simple cubic (SC) one in which the cells' centers are located on the vertices of the cubic unit cell. In the second arrangement, the face-centered cubic (FCC) one, there are cells at the vertices and the centers of the faces of the cube.

The resulting variation in the average radial concentration profile of MNPs around the center of a particular cell is shown in figure 8. All data in figure 8 correspond to the cell dimensions used in the work of (Lin *et al* 2015). The black and green lines in figure 8(a) correspond to the FCC and SC arrangements of cells, respectively, and relate to the case that the MNPs are uniformly distributed within the cells with no MNPs in interstitial regions. The blue and red lines are the corresponding average concentrations when the MNPs are only in the cell nuclei. The horizontal dashed lines show the surrogate concentration profiles, with constant values corresponding to the packing densities of the spheres as listed in table 2. These constant concentrations outside the considered cell will be used below to estimate the overall dosimetric effect from a concentration of MNPs.

Figure 8(a) shows the relative concentrations of MNPs for the four cases up to a value of r_i/R_n of 30 as solid lines. The concentrations have been normalized to the density in the nucleus of the considered cell. The dashed lines represent the packing density (volume fraction) of cells or nuclei and correspond to the large-scale average concentration of MNPs. These constant values also apply to all larger radial distances (up to potential boundaries of the region loaded with MNPs). The data suggest that for complete uptake of the MNPs into the cells at constant intracellular concentration, the average concentration of MNPs outside the cell would be 52% or 74% of the concentration in the cells, depending on the cell packing density. If the MNPs are only present in the nuclei, the effective concentration outside the considered cell decreases to 10% and 14% of the concentration inside for SC and FCC packing of the cells, respectively.

Cases 5 and 6 (see Supplementary figure 3(c) and table 1) assume that the nuclear membrane hinders diffusion of MNPs, so that there is a lower concentration of MNPs in the nucleus than in the cytoplasm. In case 5, the average cellular concentration is the same as outside the cell, in case 6 it is only 50% of that concentration. The concentration profile that corresponds to case 5 for an FCC arrangement of the cells is shown as the black line in figure 8(b); the corresponding concentration profile for scenario 6 is shown as the purple line in figure 8(b). It should be noted

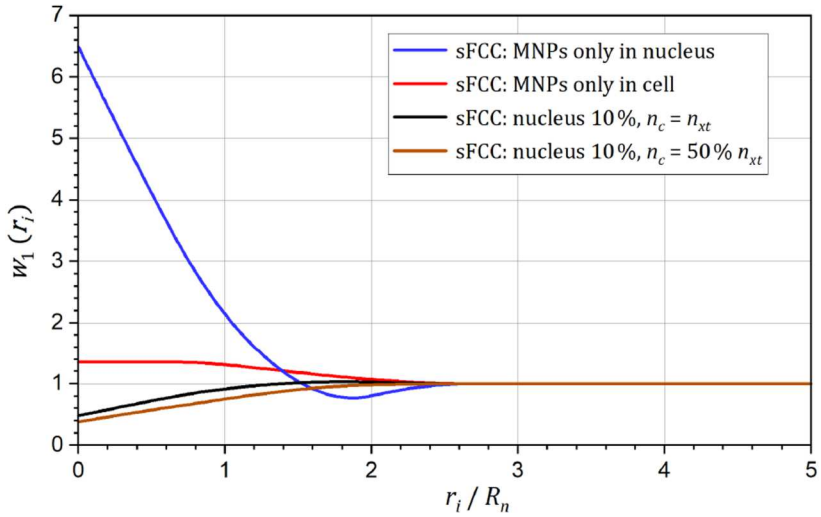


Figure 9. Weighting function for calculating the mean contribution per emitting MNP to the dose in the spherical cell nucleus (radius R_n) from the radial dose distribution (as a function of r_i) around a single MNP for the case of the surrogate MNP distribution for cells that are densely packed in an FCC lattice. The different curves apply to the following situations: MNPs only in the nuclei (blue); MNPs only in the cells (red); same concentration of MNPs in the cells and extracellular medium, but only 10% of the MNPs internalized in cells are inside the nucleus (black); the concentration in the extracellular medium is twice the average concentration inside the cells, and only 10% of the internalized MNPs are in the nucleus. The ratio of the radii of the spherical cells to those of the concentric spherical nuclei corresponds to the cell geometry employed by (Lin *et al* 2015).

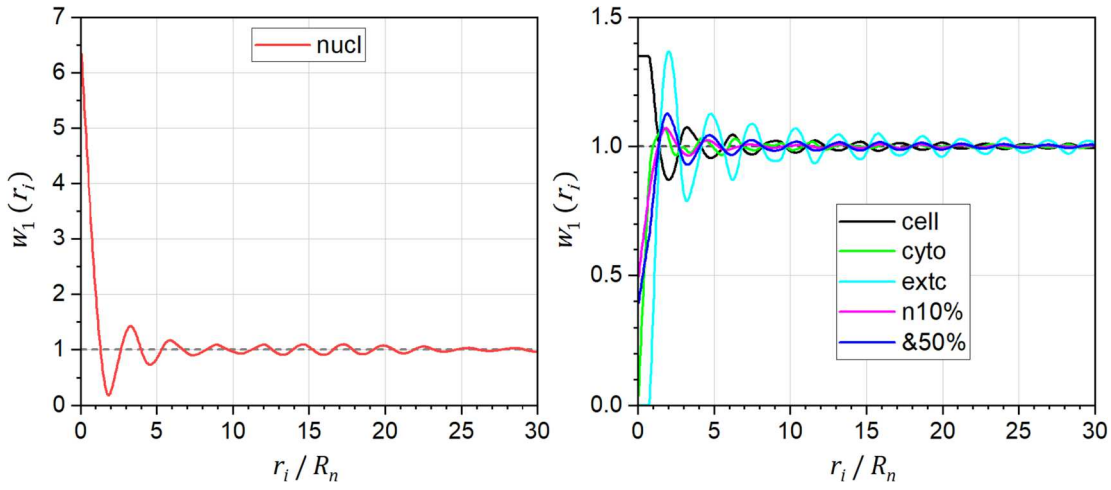


Figure 10. Weighting function for calculating the contribution per emitting MNP to the mean dose in the spherical cell nucleus (radius R_n) from the radial dose distribution (as a function of r_i) around a single MNP for cells that are densely packed in an FCC lattice. The curves apply to the first six uptake scenarios in table 1. (a) MNPs only in the nuclei; (b) MNPs uniformly distributed in the cells (black); MNPs uniformly distributed in the cytoplasm (green); MNPs only in extracellular medium (cyan); same concentration of MNPs in the cells and extracellular medium, but only 10% of the MNPs internalized in cells are inside the nucleus (magenta); the concentration in the extracellular medium is twice the average concentration inside the cells, and only 10% of the internalized MNPs are in the nucleus (blue). The ratio of the radii of the spherical cells to those of the concentric spherical nuclei corresponds to the cell geometry employed by (Lin *et al* 2015).

that in figure 8(b), the concentration is normalized to the maximum concentration, which occurs at the cell surface. When the average concentration in the cell is the same as outside and only 10% of internalized MNPs are in the cell nucleus, the global average MNP density is about 10% lower than the maximum density. When the concentration in the cell is only 50% of that in the extracellular medium, the average concentration (purple dashed line in figure 8(b)) is only about 62% of the maximum value. In the nucleus of the considered cell, the relative MNP concentration is significantly higher than 0.1. This is because the scenario assumes 10% of the internalized MNPs to be in the nucleus, while the volume of the nucleus is about 20% of the cell volume for the geometry considered. Therefore, the concentration in the nucleus is about 50% of the concentration outside. (It is not exactly 50% because the concentration in the cytoplasm must be slightly increased to have the required average density in the cell).

The resulting weighting functions for the surrogate concentration profiles pertaining to FCC packing

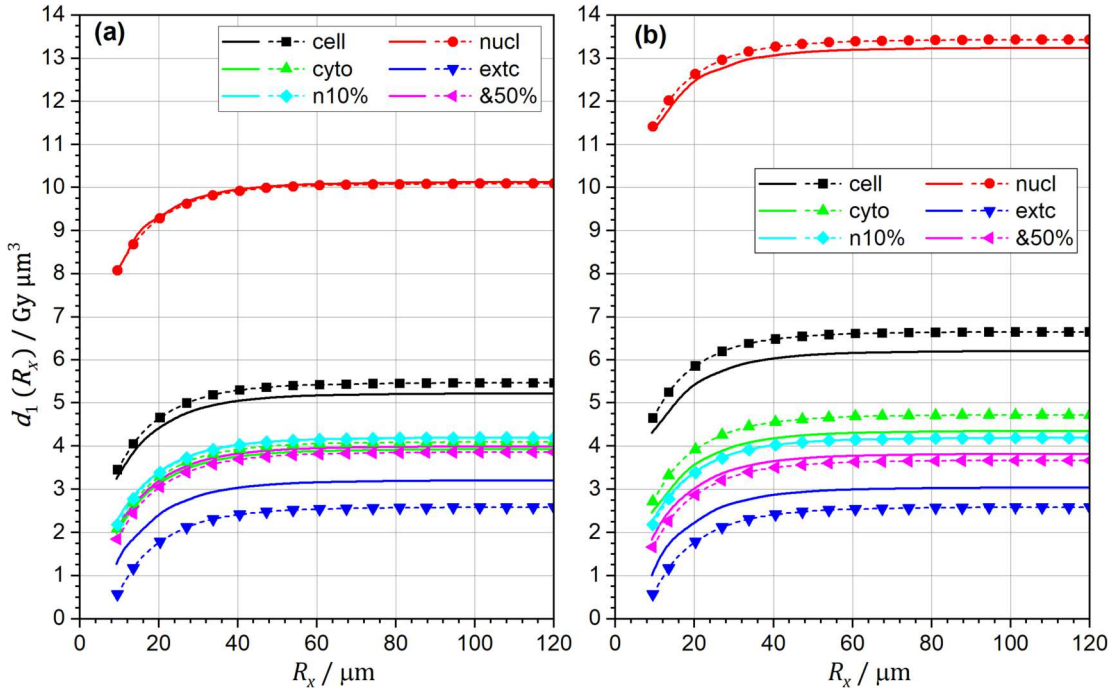


Figure 11. Contribution per emitting MNP concentration to the mean dose in the cell nucleus for different upper radius values R_x used in the determination of the weighting function for the MNP density distributions (lines) and their surrogates (symbols) as shown in figures 8(a) and (b) pertain to full MNP uptake into the nuclei, (c) and (d) pertain to the uptake scenarios 2 to 6 in table 1 (see legends). (a) and (c) are for FCC packing of cells, and (b) and (d) are for SC packing. The data apply to the dose distribution (shown in Supplementary figure 6) around a 50 nm gold MNP that is irradiated with a mixed photon and electron field originating from a 100 kVp x-ray photon spectrum from (Thomas *et al* 2024).

are shown in figure 9. The corresponding data for SC packing can be seen in Supplementary figure 4. As would be intuitively expected, radial distances exceeding the nuclear radius or the cellular radius receive a significantly higher weight than small radial distances for the concentration profiles shown in figure 8(b), i.e., when there is reduced uptake of the MNPs by the cells or the cell nucleus. For enhanced uptake into the cells, there is more weight given to the dose at a small distance from the MNP.

3.4. Comparison of the FCC and SC concentration profiles with the respective surrogates

The MNP concentration profiles of the FCC and SC arrangements of cells deviate significantly from the dashed lines in figure 8. The corresponding weighting functions have been obtained based on the approach presented in appendix A6. Those for the FCC cell arrangement are displayed in figure 10 for the first six scenarios for MNP uptake into the cells (see table 1).

The weighting functions in figure 10 have a much smoother appearance than the density profiles in figure 8, but they still show significant oscillations where the crests reflect the coordination shells. The weighting functions oscillate around unity at radial distances from the MNP exceeding the cell radius, because the average MNP concentration is identical to the values indicated by the dashed horizontal lines.

The bias introduced by using the surrogate weighting functions instead of those shown in figure 10 is illustrated in figure 11. This figure shows the contribution to the mean dose in the nucleus per average MNP concentration, $\overline{d_1}(R_n, R_c, R_x, u_n, u_p, u_x)$ (equation (A22)), as a function of the radius of the outermost sphere representing the MNP-containing region around the considered cell for the first six uptake scenarios in table 1. The colors indicate the uptake scenario (see legends), the symbols represent the results obtained using the surrogate MNP concentration outside the cell shown as dashed lines in figure 8. The solid lines are the corresponding results based on the weighting function shown in figure 10 and Supplementary figure 5, where figure 11(a) relates to the FCC arrangement of cells and figure 11(b) to the SC packing.

It can be seen that there appears to be almost no bias for the case of full MNP uptake into the nuclei in FCC-packed cells (figure 11(a)) and only a small bias for SC-packed cells (figure 11(b)). Larger offsets can be seen in figures 11(a) and (b) for the other scenarios with both packing densities of cells. In the case of no uptake into the cells (dark blue symbols and lines), the discrepancy is in the order of 20%. However, there seems to be an offset rather than a variation of the discrepancy with the value of the upper integration limit. This suggests that the discrepancy is already accumulated in the vicinity of the cell surface where the weighting functions show the highest oscillations (figure 10) and the deviations between the actual and surrogate concentrations are largest (see figure 8).

This indicates that the deviations seen in figures 11(a) and (b) could be reduced by using additional spherical shells around the sphere representing the cell to better approximate the concentration profiles shown as solid lines in figure 8. On the other hand, cells in tissue do not form a crystal lattice, so that the two cases of FCC and SC packing and their surrogates are only an estimate of the situation that would be found with real cells in real tissue. The difference between the two packing densities amounts to almost 35% in the case of complete uptake into the nucleus (red curves and symbols infigures 11(a) and (b)). For MNPs uniformly distributed in cells (black-curves and symbols in figures 11(a) and (b)), the difference is in the order of 10%, and only for the 'mixed' cases with reduced MNP uptake in the cell nuclei do the differences appear to be in the range of a few percent.

4. Discussion

4.1. Key features of the presented approach

An approach is presented that allows calculation of the mean and variance of the dose in a cell nucleus from the dose resulting from the emission of particles from an MNP undergoing an ionizing radiation interaction or decay. The approach is based on weighting functions derived from the concentration profile of MNPs around the cell under consideration, which are dimensionless and depend parametrically on the geometry and the relative concentration of the MNPs in different regions of the geometry. The actual dosimetric effects produced by a given MNP distribution are the sums of terms scaling with the average number density of emitting MNPs, $\bar{n}_a$, or its square (equation (29)). The factors scaled by $\bar{n}_a$ and $\bar{n}_a{}^2$ are weighted averages of the radial distribution of the dose contribution from a single emitting MNP or of a quadratic form (bilinear combination) of this radial dose distribution.

The corresponding results are expectation-true estimates of the quantities considered, and their estimated uncertainties can be determined by using the same weighting functions, following the Guide to the Expression of Uncertainty in Measurements (JCGM 2008). Determining the uncertainties could, in principle, also be achieved by Monte Carlo techniques. However, to the authors' knowledge, all studies determining the dose effects of MNPs based on the LEM have only simulated the dose in the cell nucleus for one configuration of a set number of randomly distributed MNPs. That is, only for a single sample of the distribution of positions. Assessing the contribution to the uncertainty resulting from different sets of MNP positions would require multiple such simulations, which may become challenging in terms of computation time.

4.1.1. Required input data

To apply the weighting functions, the dose distribution from particles emitted upon an ionizing interaction (or a decay) occurring in the MNP is needed. To determine this quantity, several authors, such as (Lin *et al* 2015), first simulated the radiation interaction with an MNP in a vacuum to obtain the fluence of emitted secondary particles. The latter was then used as input for a second simulation step to determine the contribution of the emitted particles to the dose around the MNP. (Li *et al* 2020, 2024) simulated an MNP in water irradiated by a confined beam. The difference between the results obtained with the MNP and without can be used as an estimate of the contribution of an ionizing interaction in the MNP to the dose around it (Rabus *et al* 2019, 2020).

A similar approach was used by (McMahon *et al* 2011a) and (Thomas *et al* 2024), with the difference that in a precursor simulation, the fluence of photons and electrons impinging upon the MNP was determined as input for the simulation of the radiation interaction and ensuing dose deposition around the MNP. In (Thomas *et al* 2024), these two further steps were determined in the same simulation, so that again, the difference between the results in the presence and absence of the MNP must be used as surrogate for the dose produced by particles emerging from the MNP as a result of an ionization occurring within it. As will be shown in the second part of the paper, the fact that (Thomas *et al* 2024) determined imparted energy separately for the cases of incident photons and electrons and for emitted electrons and photons allows this drawback to be remedied.

The best dataset for use with the weighting functions is obtained when two conditions are met. First, the fluence impinging on the MNP is determined in a precursor simulation, such as in (Thomas *et al* 2024), and this fluence—and not the fluence of the primary beam—is used in the next step. Second, in the next step, it is assured that the contribution from interactions in the MNP is separated from the contributions due to interactions in water of the incident particles that have not interacted in the MNP. This can be achieved by a two-step approach like the one used by (Lin *et al* 2015). Alternatively, the histories of primary particles leaving the MNP can simply be terminated in the simulation. With data obtained in this way also for a water nanoparticle instead of a MNP, it is possible to use the weighting functions to determine the dose contribution from all water nanoparticles present in a geometry without need for obtaining this information by a separate simulation (as in (Thomas *et al* 2024)) or by reference to literature data (as in (Rabus *et al* 2021b)).

A further condition placed on the dataset is that it covers the complete radial range in which energy is imparted by particles emitted by the MNP or their descendants. For the data of (Thomas *et al* 2024), this is the case, as can be seen in Supplementary figure 7.

Supplementary figure 7(a) shows that the energy imparted per radial interval tends toward zero at the highest radial distances used for scoring. Consequently, the curves of the cumulative energy imparted in spheres of increasing radius around the emitter show saturation behavior.

Since the weighting functions are purely geometrical, they are generally applicable for any type of primary particle and energy spectrum. The key requirement is that the radial dose distribution around an MNP is known. In situations where there are large changes in the fluence spectrum within the radiation field over the region of interest (Rasouli *et al* 2019), application of the approach may require simulation results of the dose around an MNP for different locations within the region of interest. This is not a caveat of the approach presented here but rather of the input data that is needed. It should also be noted that the weighting functions do not depend on the MNP size, while their application to obtain the contributions to the mean dose and mean square of the dose involves an integral over the radial dose distribution around the MNP that has the radius of the MNP as its lower limit. Investigating the dependence of the results on this parameter is one of the questions that will be addressed in the second part of the paper.

4.2. Comparison with the approach of Melo-Bernal *et al*

The first and most important difference to the approach taken by (Melo-Bernal *et al* 2021) is the different perspective taken as a starting point. Melo-Bernal *et al* considered the part of the dose distribution around a given MNP that falls inside a region such as a cell or a cell nucleus. Here, the initial question was, how many MNPs at a given distance from a considered point inside the scoring region contribute to the dose at this point? The latter perspective allows determination of the dose at different radial distances from the center of the nucleus. When the mean dose or mean square of the dose from a single MNP is determined, both approaches are equivalent and give the same results. However, the approach presented here also allows determination of the synergistic contribution from pairs of MNPs to the mean square of the dose in the nucleus.

In the approach of (Melo-Bernal *et al* 2021), the synergistic contribution from pairs of MNPs cannot easily be assessed, and Melo-Bernal *et al* argued that it is negligible, given the low probability of radiation interaction within a MNP. However, equation (23) shows that the synergistic contribution varies with the square of the MNP concentration, like the square of the mean dose. As can be seen in figure 4, the weighting function for the difference between the synergistic term and the square of the mean dose has very small values compared to the weighting function for the synergistic term shown in figure 3. This means that the variance of the dose in the nucleus is essentially given by the contribution to the mean square of the dose from single MNPs, $\overline{D_{Ns}^2}$, which is proportional to the MNP concentration, as is the contribution to the mean of the dose from MNPs, $\overline{D_N}$.

However, this does not imply that the approximation of neglecting the synergistic term made by Melo-Bernal *et al* was justified. On the contrary, when the synergistic term is neglected, the mean square of the dose is underestimated. This is because the synergistic term is approximately the same as the square of the mean dose which is responsible for the nonlinear part of the logarithm of survival probability.

A second difference is that the weighting functions determined here parametrize geometry and the uptake scenario and can be readily used with data produced by any studies determining the radial dependence of the dose contribution from an emitting MNP. They can also be easily coupled with parameterizations of the radial dose distribution, such as was done in (Melo-Bernal *et al* 2021). However, the assumption that the radial dependence of the dose distribution around an MNP can be described by a power law is a very rough approximation, as can be seen in Supplementary figure 6. In this figure, the data used to produce the results in figures 7 and 11 are displayed as the product of dose and radius squared, i.e., as the quantity to which the weighting functions are applied in equations (19) and (22). It is evident that the curve plotted in Supplementary figure 6 (in a log–log representation) is not well represented by a straight line.

Further differences are that the present approach involves a transparent separation of the overall quantitative effect, encoded by the average number density of emitting MNPs[5], the relative effects related to geometry and uptake scenario, and the specific dose distribution around an emitting MNP. The radial dose distribution around a single emitting MNP depends on the MNP radius and radiation quality. The corresponding weighted quantities $\overline{d_1}(R_c)$ (equation (19)), $\overline{d_1^2}(R_c)$ (equation (22)), and $\overline{d_2^2}(R_c)$ (equation (24)) for a uniform MNP distribution in a sphere of radius R_c depend parametrically on the radius r_p of the MNP and the ratio of R_c to the radius R_n of the cell nucleus. They do not depend on the average concentration of emitting MNPs. The resulting quantities for an uptake scenario (equation (29)) are linear or bilinear combinations of these elementary weighted dose quantities. They depend on

[5] The average number density $\bar{n}_a$ of emitting MNPs may appear to be a somewhat unimaginative concept. In principle, it could be replaced by the product of $\bar{n}_a$ and the cell or nucleus volume. In which case the resulting reference quantity would be the ratio of the number of emitting MNPs to the number of cells or nuclei. Or the mean number of emitting MNPs per cell or cell nucleus but without them necessarily being present in the cell or the nucleus (depending on uptake scenario). While this may be more imaginative, correctly phrasing what this reference quantity is exactly appeared a bit cumbersome.

radiation quality as well as MNP radius, geometry, and relative concentrations, but they do not depend on the absolute concentration of emitting MNPs. It must be noted, however, that the density of emitting MNPs is determined by the concentration of the MNPs and the expected number of interactions per MNP (equation (8)). For external irradiation, the latter depends on MNP size, the radiation quality, and fluence; for radioactive MNPs, they depend only on the activity per MNP and the exposure time.

4.3. Relevance

The surrogate model of a sphere plus two concentric shells is a generalization of approaches in the literature to assess the impact of MNPs on the survival of cells within the framework of the LEM (e.g., (Lin *et al* 2015)). It was shown to approximate the case of cells in tissue reasonably well. Regarding the effects of MNPs in different uptake scenarios, it was shown that in contrast to cases with complete uptake of MNPs by cells (figure 5), the weighting functions for incomplete uptake scenarios show large differences between isolated cells and cells in solution (figure 6). For *in vitro* studies of cells and incomplete uptake of MNPs by the cells, the background concentration of MNPs in the solvent can therefore have a significant effect on the mean dose in the cell nucleus. With the data shown in figure 7, this effect translates into a factor of between 2 and 5 for the considered radiation quality and uptake scenarios. This implies that for these cases, there is an underestimation of the lesions resulting from the linear term of the LQ model by a factor of 2 to 5 and of the lesions according to the square term by a factor of 4 to 25! And this is even without considering the LEM-specific additional lesions due to the dose non-uniformity.

For scenarios with complete uptake of the MNPs by cells, figure 7 showed no significant influence of the environment when the cells are in solution. However, for cells in tissue there is a significant contribution to the mean dose in a considered cell due to MNPs emitting in neighboring cells. This contribution amounts up to several 10% (figure 11). For incomplete uptake scenarios, similar factors are obtained as with cells in solution. Comparison of figures 11(a) and (b) shows that different packing densities of cells also result in changes in the order of up to several 10%. It will be interesting to explore how these differences affect the predicted survival curves. This will be investigated in the second part of the paper.

4.4. Impact of the approximations implied

Several approximations were implicitly made in the approach (and in that of (Melo-Bernal *et al* 2021)). One is that the contribution of an MNP to the dose in its vicinity has spherical symmetry. (Derrien *et al* 2023) reported an anisotropy of energy imparted around a spherical MNP amounting to several 10% for monoenergetic photons with a simulation setup that did not assure charged particle equilibrium (CPE). (Rabus 2024a) showed that after correction for CPE, the anisotropy was reduced to below 4% for the extreme cases reported by (Derrien *et al* 2023). (Rabus 2024a) also pointed out that this non-isotropy may, to some extent, be a simulation artefact, since some radiation transport codes model photoemission from all atomic shells according to Sauter's formalism, which strictly only applies to K shells.

A second assumption is that the radial dose distribution around an MNP does not change in the presence of other MNPs. In the study of (Thomas *et al* 2024), it was found that for electrons impinging upon MNPs, the fluence of outgoing electrons is only slightly different from that of incident electrons, with a minor reduction in the percent range at energies higher than 1 keV. At kinetic energies below 100 eV, a reduction of about 50% was found. But these electrons are stopped within tens of nanometers and can therefore be ignored. Higher-energy electrons (energies of several tens of keV) have ranges of 50 μm or higher and may therefore interact with multiple MNPs.

Since elastic electron scattering occurs predominantly in the forward direction, elastic collisions will not lead to major distortions of the spatial distribution of energy transfer points. However, the small energy losses caused by impact ionization interactions with MNPs will accumulate and may lead to a reduction in the electron range. At the same time, there is also production of bremsstrahlung photons, which will carry their energy over longer distances than electrons would. The mentioned effects may lead to a change in the radial dose profile which can presumably be treated as a small uncertainty. However, this must be confirmed in further studies which could, e.g., simulate the dose distribution around an MNP immersed in uniform mixtures of water and the MNP material at different concentrations of the latter.

Another approximation was the use of the LQ model instead of the LQL model of cell survival. This leads to an overestimation of the number of induced lesions owing to the contribution from emitting MNPs located in the nucleus (equation (5)). This effect is not expected to be large. Using the weighting functions for the radial dose profile in the cell nucleus, it is possible to calculate the quantity defined in equation (6) for given radial distance from the nucleus center after evaluating the expected dose according to equation (16). However, this is more involved, since it requires determination of the dose profile for a specific scenario and the average number density of emitting MNPs. Therefore, addressing this point is postponed until future work.

Finally, the approach assumes that the cell nucleus is a sphere and that the MNPs have a spherical symmetric distribution, thus also implying that cells are spherical. Cells are generally not

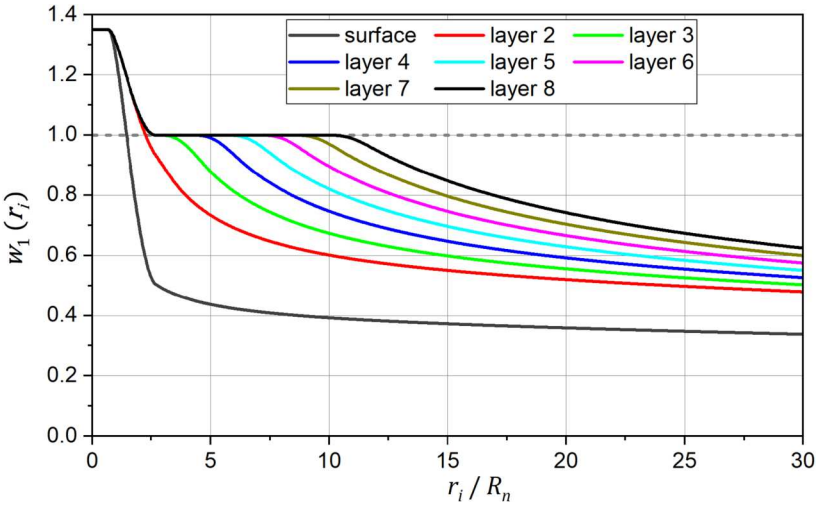


Figure 12. Modified weighting functions for the sFCC case (cf table 2) and complete uptake into the cells for cells located near the surface of a spherical tumor of 1 mm diameter. The dark gray curve corresponds to cells directly at the surface, the colored curves correspond to cells at between two and eight cell layers from the tumor surface (see legend).

spheres, and studies have shown that the choice of cellular geometry has an impact on the dose to the cell nucleus in the presence of MNPs (Sung *et al* 2017). Similarly, scenario 8, presented as a surrogate for the situation of MNPs clustered inside an endosome, appears far from realistic, since endosomes are generally not in the form of a spherical shell. Another obvious over-idealization was assuming cells to be arranged in a simple cubic or face-centered cubic lattice like atoms or ions in a crystal. However, for the latter case of cells in tissue, it was shown that the ideal arrangement of cells can be approximated by a surrogate concentration profile for the MNPs with a constant value in the extracellular region. The value of the constant depends on the average density of cells only and not on their exact arrangement. If the cells are randomly distributed within a certain range around the ideal lattice points, the system will be amorphous, and the oscillations seen in figures 8 and 9 with the radial density profile and the resulting weighting function will be smeared out and dampened away.

With the case of MNPs in the endosome, a similar approach of angular averaging of the MNP density can be applied by determining the solid angle of a sphere of radius r_i around a point in the nucleus according to equation (16). The key point here is that the weighting functions refer only to radial distances. Leaving aside synergistic effects that have been reported for MNP clusters (Rudek *et al* 2019), it should not matter for the dose to the nucleus whether the MNPs are concentrated in a small volume or are smeared out over the spherical shell defined by the MNPs closest and farthest from the center of the nucleus. In the latter case, the larger solid angle and value of the weighting function is compensated by the reduction in MNP density. Therefore, only the assumption of a uniform density in the spherical shell may be questioned. Given the insight from the case of cells in tissue, it can be expected that a surrogate concentration profile with a constant value may also give a reasonably adequate approximation in this case. This conjecture can be confirmed by using a similar approach as for cells in tissue and is left for future work.

Another caveat to be mentioned is that for the case of cells in tissue, it was implicitly assumed that all cells would be surrounded by cells containing the same concentration of MNPs and that these cells would therefore have the same expectations for the mean and standard deviation of the dose. However, there may be a distribution of the mean and standard deviation of the dose per cell. For instance, in a tumor uniformly loaded with MNPs, the cells near the surface have a lower coordination number of neighbors containing MNPs and, therefore, have a lower mean dose than cells in the inner of the tumor. There also could be a gradient from the surface inward owing to hampered uptake (like as happens with hypoxia).

As was pointed out by (Zygmanski *et al* 2013), a non-uniform dose distribution in a cell population will lead to modifications of cell survival fractions. However, these cases can also be approximately addressed by the formalism discussed in this paper. As an illustration, figure 12 shows the modified weighting functions for cells located at between one and eight cell layers from the surface of a spherical tumor, assuming the surrogate case of densely packed cells and MNPs uniformly distributed within the cells. For the cells at the surface, the weighting factor outside of the cell is significantly lower than unity for all radial distances larger than the cell radius. The same applies to the second layer. Starting with the third layer, a plateau appears in which the weighting function is unity

until it finally starts to drop (when the distance from the center of the considered cell exceeds its distance from the surface). This assessment relies on the generalized weighting functions given in appendix A6.

5. Conclusions

An approach has been presented that allows calculation of the mean dose and variance of the dose in a cell nucleus from the radial distribution of the additional dose around an MNP undergoing an ionizing interaction or radioactive decay. The methodology is based on the probability of finding MNPs at a given distance from a point at which the dose is evaluated. With this different perspective, it also became possible to assess the synergistic contribution of pairs of MNPs to the variance of the dose. It could be shown that this contribution is of similar magnitude to the square of the mean dose and therefore cannot be neglected as was done in the previous study of (Melo-Bernal *et al* 2021). The weighting functions for several surrogate cases have been explicitly stated in the appendix and can be used by other researchers to assess cell survival according to the LEM from their simulations of the dose around single MNPs. Based on the weighting function, conclusions could be drawn regarding the suitability of model cases of isolated cells in a spatially confined distribution of MNPs. It could be shown that for complete uptake scenarios and cells in solution, such simple cases can be used, whereas for partial uptake scenarios or cells in tissue, the presence of MNPs in an extended environment cannot be ignored. The extent of this environment is defined by the radial range within which the particles emitted by an MNP impart their energy. The case of a sphere and two surrounding spherical shells with constant MNP concentration in each but different between these regions has been suggested as a surrogate model for cells in tissue and shown to approximate to within a few 10% the results obtained with an idealized exact placement of the cells in a regular lattice. Similar deviations were found between different packing densities of cells. The approach presented here will be used in the second part of the paper to derive predictions of cell survival based on the LEM for different radiation qualities and uptake scenarios.

Acknowledgments

LT acknowledges support by the Metrology for Artificial Intelligence in Medicine (M4AIM) program which was funded by the German Federal Ministry for Economy and Energy in the frame of the QI Digital initiative. The authors thank Christian Velten for his comments on an earlier version of this manuscript, and Piotr Zygmanski and Wolfgang Hoegele for an interesting discussion on their approach to handling the stochastic effects with nanoparticles.

Data availability statement

All data that support the findings of this study are included within the article (and any supplementary files).

Appendix

A1. Analytical expression for the monovariate weighting function

The weighting function $\bar{\omega}(r_i|R_c)$ for the dose at a radial distance r_i from the MNP used to obtain the mean dose in the cell nucleus from a uniform distribution of MNPs in a sphere of radius R_c is given by equations (A1):

$$\bar{\omega}(r_i|R_c) = \bar{\omega}_1(x_i|a) = \begin{cases} 1 & x_i \leqslant a-1 \\ \bar{\omega}_1{}^{(2)}(x_i|a) & a-1 \leqslant x_i \leqslant a+1 \\ 0 & x_i > a+1 \end{cases} \tag{A1}$$

Here, the reduced quantities given by equation (A2) have been used:

$$x_i = \frac{r_i}{R_n};\ a = \frac{R_c}{R_n} \tag{A2}$$

The function $\bar{\omega}_1{}^{(2)}$ is given by equation (A3):

$$\bar{\omega}_1{}^{(2)}(x_i|a) = \frac{1}{2}(1+a^3) - \frac{3}{8}(1+a^2)x_i + \frac{1}{16}{x_i}^3 - \frac{3}{16}(1-a^2)^2 x_i^{-1} \tag{A3}$$

A2. Analytical expression for the bivariate weighting function $\bar{\omega}_2$

The analytical expression of the weighting function $\bar{\omega}_2$ (for the derivation see section S1.3 of Supplement 1) is given by equation (A4) using the reduced quantities defined by equation (A5):

$$\bar{\omega}_2(r_i, r_j|R_c) = \begin{cases} \bar{\omega}_1(x_i|a) & x_j \leqslant a-1 \leqslant x_i \leqslant a+1 \\ \bar{\omega}_2{}^{(3)}(x_i, x_j|a) & a-1 \leqslant x_j \leqslant 2a-x_i \wedge x_j \leqslant x_i \leqslant a+1 \\ \bar{\omega}_2{}^{(4)}(x_i, x_j|a) & 2a-x_i \leqslant x_j \leqslant x_i \leqslant a+1 \\ 0 & x_i \geqslant x_j > a+1 \end{cases} \tag{A4}$$

Table A1. Coefficients of the polynomials $P_3^{(3)}(x_j|a)$, $P_4^{(3)}(x_j)$, and $P_5^{(3)}(x_j|a)$ in equation (A6).

	$P_3^{(3)}$	$P_4^{(3)}$	$P_5^{(3)}$
x_j^0	$\frac{(a-1)^2(2a+1)}{16}$	0	$-\frac{(a-1)^3(8a^2+9a+3)}{80}$
x_j^1	$\frac{3}{16}(1-a^2)$	$-\frac{1}{8}$	$\frac{3}{32}(a^2-1)^2$
x_j^2	$\frac{3}{16}$	0	$\frac{1}{16}(a-1)^2(2a+1)$
x_j^3	$\frac{1}{16}$	$\frac{1}{160}$	0

Table A2. Coefficients of the polynomials $P_3^{(4)}(x_i|a)$, $P_4^{(4)}(x_i|a)$, and $P_5^{(4)}(x_i|a)$ in equation (A7).

	$P_3^{(4)}$	$P_4^{(4)}$	$P_5^{(4)}$
x_i^0	0	$\frac{(1-a^2-a^3)}{16}$	$-\frac{(8a^5+15a^4-a^2+3)}{80}$
x_i^1	$-\frac{1}{8}$	$-\frac{3}{16}(1-a^2)$	$-\frac{3}{32}(a^2-1)^2$
x_i^2	0	$\frac{3}{16}$	$\frac{(1-a^2-a^3)}{16}$
x_i^3	$-\frac{1}{160}$	$-\frac{1}{16}$	$-\frac{1}{8}$

$$a = \frac{R_c}{R_n};\ x_i = \frac{\max(r_i, r_j)}{R_n};\ x_j = \frac{\min(r_i, r_j)}{R_n} \quad \text{(A5)}$$

The functions $\bar{\omega}_1$, $\bar{\omega}_2^{(3)}$, and $\bar{\omega}_2^{(4)}$ appearing in equation (A4) are given by equations (A1), (A6), and (A7), respectively:

$$\bar{\omega}_2^{(3)}(x_i, x_j) = \bar{\omega}(x_i) + \frac{1}{2}\bar{\omega}(x_j) - \frac{1}{2} + \frac{x_i}{x_j}P_3^{(3)}(x_j|a) + \frac{x_j}{x_i}P_4^{(3)}(x_j) + \frac{1}{x_i x_j}P_5^{(3)}(x_j|a) \quad \text{(A6)}$$

$$\bar{\omega}_2^{(4)}(x_i, x_j) = \frac{1}{2}\bar{\omega}(x_i) + \frac{x_i}{x_j}P_3^{(4)}(x_i) + \frac{x_j}{x_i}P_4^{(4)}(x_i|a) + \frac{1}{x_i x_j}P_5^{(4)}(x_i|a) \quad \text{(A7)}$$

$P_k^{(3)}(x_j|a)$ and $P_k^{(4)}(x_i|a)$ $(k \in \{3, 4, 5\})$ are polynomials of third degree in the first argument. The polynomial coefficients depend on the parameter a and are listed in tables A1 and A2.

A3. MNPs uniformly distributed in a spherical shell only

Since the dose from different sources is additive, the weighting functions for the radial dose distribution in the nucleus and for the mean dose in the nucleus are easily obtained from equations (16) and (19). The adjusted formulas for MNPs inside a spherical shell of inner radius R_n and outer radius R_c only are given by equations (A8) and (A9):

$$D(\vec{r}) = D_w + \bar{n}_m \int_{r_p}^{\infty} D_1(r_i)[\Omega(r_i, r|R_c) - \Omega(r_i, r|R_n)]\, r_i^2 dr_i \quad \text{(A8)}$$

$$\bar{D}(R_n, R_c) = D_w + \bar{n}_m\,[\overline{d_1}(R_c) - \overline{d_1}(R_n)] \quad \text{(A9)}$$

Here, $\bar{n}_m$ is the number density of MNPs in the spherical shell, and $\overline{d_1}(R_n)$ and $\overline{d_1}(R_c)$ are the dose contributions per number density of emitting MNPs corresponding to spheres of radius R_n and R_c, respectively (given by equation (18)).

The average contribution of a single MNP to the mean square of the dose can be calculated in the same manner as the last term in equation (A9) by substituting $\overline{d_1^2}$ for $\overline{d_1}$.

However, for the mixed terms in equation (24) pertaining to the synergistic contribution from pairs of MNPs to the mean square of the dose, it is not possible to simply subtract the weighting functions for the smaller sphere from those of the larger one. This is because the contribution from two MNPs within the larger sphere is the sum of the cases that (a) both MNPs are in the spherical shell, (b) both are in the inner sphere, and that (c) one of them is in the spherical shell and the other in the inner sphere.

The last contribution is given by the product of the mean doses per number density for one MNP in the spherical shell and the other in the inner sphere. This leads to equation (A10), which can be rewritten as equation (A11):

$$\begin{aligned}\overline{D_{Np}^2} &= \bar{n}_m{}^2 \times [\overline{d_2^2}(R_c) - 8V_p \times \overline{d_1^2}(R_c)] \\ &\quad - \bar{n}_m{}^2 \times [\overline{d_2^2}(R_n) - 8V_p \times \overline{d_1^2}(R_n)] \\ &\quad - 2\bar{n}_m\overline{d_1}(R_n) \times \bar{n}_m[\overline{d_1}(R_c) - \overline{d_1}(R_n)]\end{aligned} \quad \text{(A10)}$$

$$\begin{aligned}\overline{D_{Np}^2}(R_n, R_c) &= \bar{n}_m{}^2(\overline{d_2^2}(R_c) - \overline{d_2^2}(R_n) \\ &\quad - 2\overline{d_1}(R_n)[\overline{d_1}(R_c) - \overline{d_1}(R_n)]) \\ &\quad - \bar{n}_m{}^2 8V_p(\overline{d_1^2}(R_c) - \overline{d_1^2}(R_n))\end{aligned} \quad \text{(A11)}$$

A4. MNP distribution with different constant values in a sphere and a surrounding spherical shell

The case that MNPs are uniformly distributed in a sphere of radius R_n at a number density $\bar{n}_n$ and in a surrounding spherical shell at a different number density $\bar{n}_p$ could, for instance, occur if there is complete uptake of the MNPs into a cell, while the uptake into the nucleus is reduced compared to the cytoplasm. The case is also treated here as a preliminary to the generalization to a continuous variation of the number density with radial distance from the center of the cell nucleus (see appendices A6 and A7). For the case of the contribution of MNPs to the mean dose, the resulting expression is simply the sum of equation (18) and the second term on the right-hand side of equation (A9), as shown in equation (A12):

$$\bar{D} = D_w + \bar{n}_n\overline{d_1}(R_n) + \bar{n}_p[\overline{d_1}(R_c) - \overline{d_1}(R_n)] \quad \text{(A12)}$$

The contribution to the mean square of the dose from the same MNP is similarly obtained by equation

(A16), with the $\overline{d_1^2}$ given by equation (22). This results in equation (A23):

$$\overline{D_{Ns}^2} = \bar{n}_n \times \overline{d_1^2}(R_n) + \bar{n}_p \times [\overline{d_1^2}(R_c) - \overline{d_1^2}(R_n)] \tag{A13}$$

For the synergistic term originating from pairs of MNPs, the situation is a bit more complex. In addition to the contributions of the sphere (equation (24)) and the spherical shell (equation (A10)), there is a contribution due to pairs of MNPs of which one is located in the sphere and the other in the spherical shell. This leads to equation (A14), where V_n and V_c denote the volumes of the spheres of radius R_n and R_c, respectively:

$$\begin{aligned}\overline{D_{Np}^2} = {} & \bar{n}_n{}^2\overline{d_2^2}(R_n) + \bar{n}_p{}^2[\overline{d_2^2}(R_c) - \overline{d_2^2}(R_n) \\ & - 2\,\overline{d_1}(R_n)\,[\overline{d_1}(R_c) - \overline{d_1}(R_n)]] - 8V_p \\ & \times (\bar{n}_n{}^2\overline{d_1^2}(R_n) + \bar{n}_p{}^2[\overline{d_1^2}(R_c) - \overline{d_1^2}(R_n)]) \\ & + 2\bar{n}_n\bar{n}_p\overline{d_1}(R_n)\,[\overline{d_1}(R_c) - \overline{d_1}(R_n)]\end{aligned} \tag{A14}$$

The last term in equation (A14) is the synergistic term for MNP pairs in which one MNP is in the sphere and the other in the spherical shell.

A5. MNP distribution with different constant values in a sphere and two concentric spherical shells

In the case of different MNP concentrations $\bar{n}_n$, $\bar{n}_p$, and $\bar{n}_x$ in the nucleus, cytoplasm, and extracellular region, respectively, the expression for the mean dose contribution from MNPs is given by equation (A15):

$$\begin{aligned}\overline{D_N} = {} & \bar{n}_n\overline{d_1}(R_n) + \bar{n}_p[\overline{d_1}(R_c) - \overline{d_1}(R_n)] \\ & + \bar{n}_x[\overline{d_1}(R_x) - \overline{d_1}(R_c)]\end{aligned} \tag{A15}$$

The contribution to the mean square of the dose from the same MNP is similarly obtained by equation (A16), with $\overline{d_1^2}$ given by equation (22):

$$\begin{aligned}\overline{D_{Ns}^2} = {} & \bar{n}_n\overline{d_1^2}(R_n) + \bar{n}_p[\overline{d_1^2}(R_c) - \overline{d_1^2}(R_n)] \\ & + \bar{n}_x[\overline{d_1^2}(R_x) - \overline{d_1^2}(R_c)]\end{aligned} \tag{A16}$$

The synergistic term takes the rather complex form of equation (A17), where V_n, V_c, and V_x denote the volumes of the nucleus, cell, and extracellular region, respectively:

$$\begin{aligned}\overline{D_{Np}^2} = {} & \bar{n}_n{}^2\overline{d_2^2}(R_n) + \bar{n}_p{}^2(\overline{d_2^2}(R_c) - \overline{d_2^2}(R_n) - 2\overline{d_1}(R_n)[\overline{d_1}(R_c) - \overline{d_1}(R_n)]) \\ & + \bar{n}_x{}^2(\overline{d_2^2}(R_x) - \overline{d_2^2}(R_c) - 2\overline{d_1}(R_c)[\overline{d_1}(R_x) - \overline{d_1}(R_c)]) \\ & - 8V_p(\bar{n}_n{}^2\overline{d_1^2}(R_n) + \bar{n}_p{}^2[\overline{d_1^2}(R_c) - \overline{d_1^2}(R_n)]) - 8V_p\bar{n}_x{}^2[\overline{d_1^2}(R_x) - d_1^2(R_c)] \\ & + 2\bar{n}_n\bar{n}_p\overline{d_1}(R_n)[\overline{d_1}(R_c) - \overline{d_1}(R_n)] + 2\bar{n}_n\bar{n}_x\overline{d_1}(R_n)[\overline{d_1}(R_x) - \overline{d_1}(R_c)] \\ & + 2\bar{n}_p\bar{n}_x[\overline{d_1}(R_c) - \overline{d_1}(R_n)] \times [\overline{d_1}(R_x) - \overline{d_1}(R_c)]\end{aligned} \tag{A17}$$

By normalizing the three number densities appearing in equations (A15)–(A17) to the average number density $\bar{n}_a$ in the sphere of radius R_x, the relative concentrations u_n, u_p, and u_x are obtained (equation (A18)):

$$u_n = \frac{\bar{n}_n}{\bar{n}_a};\ u_p = \frac{\bar{n}_p}{\bar{n}_a};\ u_x = \frac{\bar{n}_x}{\bar{n}_a} \tag{A18}$$

Together with the radii R_n, R_c, and R_x, these three parameters characterize the uptake scenario. The set $\theta = \{R_n, R_c, R_x, u_n, u_p, u_x\}$ parameterizes new weighting functions w_1, w_2, and w_{1b}, as given by equations (A19)–(A21), respectively:

$$\begin{aligned}w_1(r_i|\theta) = {} & (u_n - u_p)\varpi(r_i|R_n) \\ & + (u_p - u_x)\varpi(r_i|R_c) + u_x\varpi(r_i|R_x)\end{aligned} \tag{A19}$$

$$\begin{aligned}w_2(r_i, r_j|\theta) = {} & [u_n{}^2 - u_p{}^2]\varpi_2(r_i, r_j|R_n) \\ & + [u_p{}^2 - u_x{}^2]\varpi_2(r_i, r_j|R_c) \\ & + u_x{}^2\varpi_2(r_i, r_j|R_x) + 2(u_n - u_p)u_p\varpi(r_i|R_n) \\ & \times (\varpi(r_j|R_c) - \varpi(r_j|R_n)) \\ & + 2(u_p - u_x)u_x\varpi(r_i|R_c)(\varpi(r_j|R_x) - \varpi(r_j|R_c)) \\ & + 2(u_n - u_p)u_x\varpi(r_i|R_n)(\varpi(r_j|R_x) - \varpi(r_j|R_c))\end{aligned} \tag{A20}$$

$$w_{1b}(r_i|\theta) = [{u_n}^2 - {u_p}^2]\bar{\omega}_1(r_i|R_n) + [{u_p}^2 - {u_x}^2]\bar{\omega}_1(r_i|R_c) + {u_x}^2\bar{\omega}_1(r_i|R_x) \quad \text{(A21)}$$

With these weighting functions, the contributions to the mean dose and mean dose squared specific to the uptake scenario are obtained by equations (A22)–(A24):

$$\overline{D_N} = \bar{n}_a\overline{d_1}(\theta) = \bar{n}_a\int_{r_p}^{\infty} D_1(r_i){r_i}^2 \times 4\pi w_1(r_i|\theta)dr_i \quad \text{(A22)}$$

$$\overline{D_{Ns}^2} = \bar{n}_a\overline{d_1^2}(\theta) = \bar{n}_a\int_{r_p}^{\infty}[D_1(r_i)]^2{r_i}^2 \times 4\pi w_1(r_i|\theta)dr_i \quad \text{(A23)}$$

$$\overline{D_{Np}^2} = {\bar{n}_a}^2 \times (\overline{d_2^2}(\theta) - 8V_p\overline{d_{1b}^2}(\theta)) \quad \text{(A24)}$$

The synergistic term of MNP pairs contributing to the mean square of the dose in the nucleus is given by equation (A25), and the correction for nonoverlapping of the two MNPs by equation (A26):

$$\overline{d_2^2}(\theta) = \int_{r_p}^{\infty}\int_{r_p}^{\infty} D_1(r_i){r_i}^2 D_1(r_j){r_j}^2 \times (4\pi)^2 w_2(r_i, r_j|\theta)dr_j dr_i \quad \text{(A25)}$$

$$\overline{d_{1b}^2}(\theta) = \int_{r_p}^{\infty}[D_1(r_i)]^2{r_i}^2 \times 4\pi w_{1b}(r_i|\theta)dr_i \quad \text{(A26)}$$

A6. Generalized weighting function for the contribution to the mean dose

From equation (A15), it is evident that considering further radial shells would simply add additional terms of the same structure as the last two. If the separation between subsequent radii is an infinitesimal increment and their number increases to infinity, then the sum becomes an integral over the radial density of MNPs, as in equation (A27):

$$\bar{D} = D_w + \bar{n}_n\overline{d_1}(R_n) + \int_{R_n}^{R_x}\bar{n}_m(R)\overline{d_1}'(R)dR \quad \text{(A27)}$$

In equation (A27), $\bar{n}_m(R)$ is the number density of emitting MNPs as a function of the radial distance from the center of the cell nucleus, and $\overline{d_1}'(R)$ is the derivative of $\overline{d_1}(R)$ with respect to R. From equation (19), this derivative is given by equation (A28):

$$\overline{d_1}'(R) = \int_{r_p}^{\infty} D_1(r_i){r_i}^2 \times 4\pi\frac{\partial\bar{\omega}(r_i|R)}{\partial R}dr_i \quad \text{(A28)}$$

The partial derivative of $\bar{\omega}(r_i|R)$ with respect to R is given by equations (A29) and (A30), where the reduced quantities $x_i = r_i/R_n$ and $a = R/R_n$ have been used:

$$\frac{\partial\bar{\omega}(r_i|R)}{\partial R} = \begin{cases}\dfrac{1}{R_n}\dfrac{\partial\bar{\omega}_1(x_i|a)}{\partial a} & a-1 \leqslant x_i \leqslant a+1\\ 0 & \text{else}\end{cases} \quad \text{(A29)}$$

$$\frac{\partial\bar{\omega}_1(x_i|a)}{\partial a} = \frac{3}{2}a^2 - \frac{3}{4}a[x_i - (1-a^2)x_i^{-1}] \quad \text{(A30)}$$

The sequence of integration can be interchanged in the double integral obtained by substituting equation (A28) into equation (A27), so that equation (A31) is obtained with $\tilde{w}_1(r_i)$ defined by equation (A32):

$$\bar{D} = D_w + \bar{n}_n\overline{d_1}(R_n) + \bar{n}_r\int_{r_p}^{\infty} D_1(r_i){r_i}^2 \times 4\pi\tilde{w}_1(r_i)dr_i \quad \text{(A31)}$$

$$\tilde{w}_1(r_i) = \int_{R_n}^{R_x}\frac{\bar{n}_m(R)}{\bar{n}_r}\frac{\partial\bar{\omega}(r_i|R)}{\partial R}dR \quad \text{(A32)}$$

The factor $\bar{n}_r$ in front of the integral in equation (A31) is the mean number density of emitting MNPs inside a chosen reference volume V_r (e.g., the cell) and was introduced for convenience to make the weighting function $w_1(r_i)$ dimensionless. The first fraction under the integral in equation (A32) gives the relative profile of the MNP concentration.

A7. Generalized weighting function for the contribution to the square of the dose

As before, the same weighting function applies to the contribution to the square of the dose from single MNPs. For the synergistic term due to pairs of MNPs, the starting point is to consider equation (A17) for the case that $R_x = R_c + dR$ is only infinitesimally larger than R_c. This leads to the following expression for the derivative of $\overline{D_{Np}^2}$ (with R_c replaced with R):

$$\overline{D_{Np}^2}'(R) = (\bar{n}_m(R))^2 \times [\bar{d}_2^{2\,\prime}(R) - 8V_p\bar{d}_1^{2\,\prime}(R)] - 2(\bar{n}_m(R))^2\,\bar{d}_1(R)\,\bar{d}_1'(R) + 2\bar{n}_m(R)\,\bar{d}_1'(R)[\bar{n}_n\bar{d}_1(R_n) + \int_{R_n}^{R}\bar{n}_m(r)\,\bar{d}_1'(r)\,dr\Big] \quad \text{(A33)}$$

Integration by parts of the integral in the last term transforms equation (A33) into equation (A34):

$$\overline{D_{NN'}^2}'(R) = (\bar{n}_m(R))^2 \times [\bar{d}_2^{2\,\prime}(R) - 8V_p\bar{d}_1^{2\,\prime}(R)] + 2\bar{n}_m(R)\,\bar{d}_1'(R) \times [\bar{n}_n - \bar{n}_m(R_n)]\bar{d}_1(R_n) - 2\bar{n}_m(R)\,\bar{d}_1'(R)\int_{R_n}^{R}\frac{d\bar{n}_m(r)}{dR}\bar{d}_1(r)\,dr \quad \text{(A34)}$$

Using the same line of argument as in the previous section, equation (A35) is obtained with the quantities $\tilde{w}_2(r_i, r_j)$ and $\tilde{w}_2(r_i, r_j)$ given by equations (A36) and (A37):

$$\begin{aligned}\overline{D_{Np}^2} = \overline{D_{Np}^2}(R_n) + \bar{n}_r{}^2 \int_{r_p}^{\infty}\int_{r_p}^{\infty} D_1(r_i)\, r_i{}^2 D_1(r_j)\, r_j{}^2 \\ \times (4\pi)^2 \tilde{w}_2(r_i, r_j)\, dr_j\, dr_i - \bar{n}_r{}^2 8V_p \int_{r_p}^{\infty} [D_1(r_i)]^2 r_i{}^2 \\ \times 4\pi \tilde{w}_3(r_i)\, dr_i + 2[\bar{n}_n - \bar{n}_m(R_n)]\, \overline{d_1}(R_n) \\ \times \bar{n}_r \int_{r_p}^{\infty} D_1(r_i)\, r_i{}^2 \times 4\pi \tilde{w}_1(r_i)\, dr_i \end{aligned} \tag{A35}$$

$$\begin{aligned}\tilde{w}_2(r_i, r_j) = \int_{R_n}^{R_x} \left(\frac{\bar{n}_m(R)}{\bar{n}_r}\right)^2 \frac{\partial \bar{\omega}_2(r_i, r_j|R)}{\partial R} dR \\ + \int_{R_n}^{R_x} \frac{\bar{n}_m(R)}{\bar{n}_r} \frac{\partial \bar{\omega}(r_i|R)}{\partial R} \int_{R_n}^{R} \frac{1}{\bar{n}_r} \frac{d\bar{n}_m(R')}{dR'} \varpi(r_j|R')\, dR' dR \end{aligned} \tag{A36}$$

$$\tilde{w}_3(r_i) = \int_{R_n}^{R_x} \left(\frac{\bar{n}_m(R)}{\bar{n}_r}\right)^2 \frac{\partial \bar{\omega}_1(r_i|R)}{\partial R} dR \tag{A37}$$

Data availability

The data that support the findings of this study are available upon reasonable request from the authors.

Author contributions

Hans Rabus 0000-0001-7700-9845
Conceptualization (lead), Data curation (lead), Formal analysis (lead), Investigation (lead), Methodology (lead), Project administration (lead), Software (equal), Supervision (lead), Validation (equal), Visualization (lead), Writing – original draft (lead), Writing – review & editing (equal)

Leo Thomas 0000-0002-2156-7298
Data curation (supporting), Formal analysis (supporting), Investigation (supporting), Software (equal), Validation (supporting), Writing – review & editing (equal)

References

Braby L A *et al* 2023 ICRU report 98, stochastic nature of radiation interactions: microdosimetry *J. ICRU* **23** 1–168

Chow J C L 2018 Recent progress in Monte Carlo simulation on gold nanoparticle radiosensitization *AIMS Biophysics* **5** 231–44

Coulter J 2012 Cell type-dependent uptake, localization, and cytotoxicity of 1.9 nm gold nanoparticles *IJN* **7** 2673

Cui L, Her S, Borst G R, Bristow R G, Jaffray D A and Allen C 2017 Radiosensitization by gold nanoparticles: will they ever make it to the clinic? *Radiother. Oncol.* **124** 344–56

Derrien J, Pauly N, Adam J-F and Reniers B 2023 Investigation of the anisotropic distribution of microdosimetric quantities in the vicinity of x-ray-irradiated gold nanoparticles *Radiat. Phys. Chem.* **213** 111232

Douglass M, Bezak E and Penfold S 2012 Development of a randomized 3D cell model for Monte Carlo microdosimetry simulations *AIP Conf. Proc.* **39** 3509–19

Hainfeld J F, Slatkin D N and Smilowitz H M 2004 The use of gold nanoparticles to enhance radiotherapy in mice *Phys. Med. Biol.* **49** N309–15

Jain S, Hirst D G and O'Sullivan J M 2012 Gold nanoparticles as novel agents for cancer therapy *Br. J. Radiol.* **85** 101–13

JCGM 2008 ISO/IEC GUIDE 98-3:2008 *Uncertainty of measurement — Part 3: Guide to the expression of uncertainty in measurement (GUM:1995)* (https://iso.org/standard/50461.html)

Kim T, Millares R H, Kim T, Eom M, Kim J and Ye S 2024 Nanoscale dosimetry for a radioisotope-labeled metal nanoparticle using MCNP6.2 and Geant4 *Med. Phys.* **51** 9290–302

Krämer M and Scholz M 2000 Treatment planning for heavy-ion radiotherapy: calculation and optimization of biologically effective dose *Phys. Med. Biol.* **45** 3319–30

Kumarasamy R V, Natarajan P M, Umapathy V R, Roy J R, Mironescu M and Palanisamy C P 2024 Clinical applications and therapeutic potentials of advanced nanoparticles: a comprehensive review on completed human clinical trials *Front. Nanotechnol.* **6** 1479993

Kuncic Z and Lacombe S 2018 Nanoparticle radio-enhancement: principles, progress and application to cancer treatment *Phys. Med. Biol.* **63** 02TR01

Li W B *et al* 2020 Corrigendum to 'Intercomparison of dose enhancement ratio and secondary electron spectra for gold nanoparticles irradiated by x-rays calculated using multiple Monte Carlo simulation codes [Phys. Med. 69 (2020) 147-163] *Phys. Medica* **80** 383–8

Li W B, Rabus H, Villagrasa C and Schuemann J 2024 *Intercomparison exercise on Monte Carlo simulations of the dose enhancement by a single gold nanoparticle under X-ray irradiation* EURADOS Report 2024-1 European Radiation Dosimetry Group (EURADOS) e.V., Neuherberg, Gemany 1–60

Lin Y, McMahon S J, Paganetti H and Schuemann J 2015 Biological modeling of gold nanoparticle enhanced radiotherapy for proton therapy *Phys. Med. Biol.* **60** 4149–68

Lin Y, McMahon S J, Scarpelli M, Paganetti H and Schuemann J 2014 Comparing gold nano-particle enhanced radiotherapy with protons, megavoltage photons and kilovoltage photons: a Monte Carlo simulation *Phys. Med. Biol.* **59** 7675–89

Martinov M P and Thomson R M 2017 Heterogeneous multiscale Monte Carlo simulations for gold nanoparticle radiosensitization *Med. Phys.* **44** 644–53

McMahon S J *et al* 2011a Nanodosimetric effects of gold nanoparticles in megavoltage radiation therapy *Radiother. Oncol.* **100** 412–6
McMahon S J *et al* 2011b Biological consequences of nanoscale energy deposition near irradiated heavy atom nanoparticles *Nat. Sci. Rep.* **1** 18
Melo-Bernal W, Chernov G, Barboza-Flores M and Chernov V 2021 Quantification of the radiosensitization effect of high-Z nanoparticles on photon irradiated cells: combining Monte Carlo simulations and an analytical approach to the local effect model *Phys. Med. Biol.* **66** 135007
Rabus H 2024a Comment on 'Investigation of the anisotropic distribution of microdosimetric quantities in the vicinity of x-ray-irradiated gold nanoparticles' by Derrien *et al.* [Radiation Physics and Chemistry 213, 111232 (2023)] *Radiat. Phys. Chem.* **416** 111466
Rabus H 2024b Comment on 'Reproducibility study of Monte Carlo simulations for nanoparticle dose enhancement and biological modeling of cell survival curves' by Velten *et al.* [Biomed Phys Eng Express 2023;9:045004] *Biomed. Phys. Eng. Express* **10** 028002
Rabus H, Gargioni E, Li W B, Nettelbeck H and Villagrasa C 2020 Corrigendum: Determining dose enhancement factors of high-Z nanoparticles from simulations where lateral secondary particle disequilibrium exists (2019 *Phys. Med. Biol.* 64 155016) *Phys. Med. Biol.* **65** 159501
Rabus H, Gargioni E, Li W, Nettelbeck and Villagrasa H C 2019 Determining dose enhancement factors of high-Z nanoparticles from simulations where lateral secondary particle disequilibrium exists *Phys. Med. Biol.* **64** 155016
Rabus H *et al* 2021a Consistency checks of results from a Monte Carlo code intercomparison for emitted electron spectra and energy deposition around a single gold nanoparticle irradiated by x-rays *Radiat. Meas.* **147** 106637
Rabus H *et al* 2021b Intercomparison of Monte Carlo calculated dose enhancement ratios for gold nanoparticles irradiated by x-rays: assessing the uncertainty and correct methodology for extended beams *Phys. Medica* **84** 241–53
Rabus H and Mkanda O M 2025 Do cell culturing influence the radiosensitizing effect of gold nanoparticles part 2: scrutinizing the methodology producing recent evidence arXiv:2506.20283[physics.med-ph] June 26, 2025
Rasouli F S, Masoudi S F and Asadi S 2019 On the importance of modeling gold nanoparticles distribution in dose-enhanced radiotherapy *IJN* **14** 5865–74
Rudek B, McNamara A, Ramos-Méndez J, Byrne H, Kuncic Z and Schuemann J 2019 Radio-enhancement by gold nanoparticles and their impact on water radiolysis for x-ray, proton and carbon-ion beams *Phys. Med. Biol.* **64** 175005
Schuemann J *et al* 2020 Roadmap for metal nanoparticles in radiation therapy: current status, translational challenges, and future directions *Phys. Med. Biol.* **65** 21RM02
Schuemann J, Berbeco R, Chithrani D B, Cho S H, Kumar R, McMahon S J, Sridhar S and Krishnan S 2016 Roadmap to clinical use of gold nanoparticles for radiation sensitization *Int. J. Radiat. Oncol. Biol. Phys.* **94** 189–205
Sung W, Ye S-J, McNamara A L, McMahon S J, Hainfeld J, Shin J, Smilowitz H M, Paganetti H and Schuemann J 2017 Correction: dependence of gold nanoparticle radiosensitization on cell geometry *Nanoscale* **9** 11338–11338
Thomas L, Schwarze M and Rabus H 2024 Radial dependence of ionization clustering around a gold nanoparticle irradiated by x-rays under charged particle equilibrium *Phys. Med. Biol.* **69** 185014
Velten C and Tomé W A 2024 Reply to comment on 'Reproducibility study of Monte Carlo simulations for nanoparticle dose enhancement and biological modeling of cell survival curves' [Biomed Phys Eng Express 2023;9:045004] *Biomed. Phys. Eng. Express* **10** 028001
Velten C and Tomé W A 2023 Reproducibility study of Monte Carlo simulations for nanoparticle dose enhancement and biological modeling of cell survival curves *Biomed. Phys. Eng. Express* **9** 045004
Xie W Z, Friedland W, Li W B, Li C Y, Oeh U, Qiu R, Li J L and Hoeschen C 2015 Simulation on the molecular radiosensitization effect of gold nanoparticles in cells irradiated by x-rays *Phys. Med. Biol.* **60** 6195
Xu X, Wu J, Dai Z, Hu R, Xie Y and Wang L 2022 Monte Carlo simulation of physical dose enhancement in core–shell magnetic gold nanoparticles with TOPAS *Front. Oncol.* **12** 992358
Zygmanski P, Hoegele W, Tsiamas P, Cifter F, Ngwa W, Berbeco R, Makrigiorgos M and Sajo E 2013 A stochastic model of cell survival for high-Z nanoparticle radiotherapy *Med. Phys.* **40** 024102
Zygmanski P and Sajo E 2016 Nanoscale radiation transport and clinical beam modeling for gold nanoparticle dose enhanced radiotherapy (GNPT) using x-rays *Br. J. Radiol.* **89** 20150200